

Cite this: *Dalton Trans.*, 2014, **43**, 5694

## Syntheses, structures and electrochemical properties of a class of 1-D double chain polyoxotungstate hybrids [H<sub>2</sub>dap]-[Cu(dap)<sub>2</sub>]<sub>0.5</sub>[Cu(dap)<sub>2</sub>(H<sub>2</sub>O)][Ln-(H<sub>2</sub>O)<sub>3</sub>(α-GeW<sub>11</sub>O<sub>39</sub>)]·3H<sub>2</sub>O<sup>†</sup>

Jun-Wei Zhao,<sup>\*a,b</sup> Yan-Zhou Li,<sup>a</sup> Fan Ji,<sup>a</sup> Jing Yuan,<sup>a</sup> Li-Juan Chen<sup>a</sup> and Guo-Yu Yang<sup>\*b</sup>

A series of novel organic–inorganic hybrid 1-D double chain germanotungstates [H<sub>2</sub>dap][Cu(dap)<sub>2</sub>]<sub>0.5</sub>[Cu(dap)<sub>2</sub>(H<sub>2</sub>O)][Ln(H<sub>2</sub>O)<sub>3</sub>(α-GeW<sub>11</sub>O<sub>39</sub>)]·3H<sub>2</sub>O [Ln = La<sup>III</sup> (**1**), Pr<sup>III</sup> (**2**), Nd<sup>III</sup> (**3**), Sm<sup>III</sup> (**4**), Eu<sup>III</sup> (**5**), Tb<sup>III</sup> (**6**), Er<sup>III</sup> (**7**)] (dap = 1,2-diaminopropane) have been hydrothermally prepared and structurally characterized by elemental analyses, powder X-ray diffraction (PXRD), IR spectra, thermogravimetric (TG) analyses, X-ray photoelectron spectroscopy (XPS) and single-crystal X-ray diffraction. The most prominent structural feature of **1–7** is that the [Ln(H<sub>2</sub>O)<sub>3</sub>(α-GeW<sub>11</sub>O<sub>39</sub>)]<sup>5-</sup> moieties are firstly connected with each other via the W–O–Ln–O–W bridges creating a 1-D {[Cu(dap)<sub>2</sub>(H<sub>2</sub>O)][Ln(H<sub>2</sub>O)<sub>3</sub>(α-GeW<sub>11</sub>O<sub>39</sub>)]}<sub>n</sub><sup>3n-</sup> polymeric chain and then two adjacent antiparallel 1-D polymeric chains are linked together through [Cu(dap)<sub>2</sub>]<sup>2+</sup> linkages giving rise to the rare organic–inorganic hybrid 1-D Cu<sup>II</sup>–Ln<sup>III</sup> heterometallic double-chain architectures. To the best of our knowledge, **1–7** represent the first 1-D double-chain Cu<sup>II</sup>–Ln<sup>III</sup> heterometallic germanotungstates. The variable-temperature magnetic susceptibilities of **2**, **4** and **7** have been investigated. Furthermore, the solid-state electrochemical and electro-catalytic properties of **3** and **4** have been measured in 0.5 mol L<sup>-1</sup> Na<sub>2</sub>SO<sub>4</sub> + H<sub>2</sub>SO<sub>4</sub> aqueous solution by entrapping them in a carbon paste electrode. **3** and **4** display apparent electro-catalytic activities for nitrite, bromate and hydrogen peroxide reduction.

Received 24th December 2013,  
Accepted 21st January 2014

DOI: 10.1039/c3dt53616e

www.rsc.org/dalton

## Introduction

Polyoxometalates (POMs) are polynuclear metal–oxo complexes with unique physical and chemical performances. The oxygen-rich surface of defect or lacunary POMs renders them excellent inorganic multidentate candidates to integrate oxophilic d- or f-block metals, giving rise to a variety of novel d- or f-block metal substituted POMs with possible applications spanning a range of domains such as materials science, electro-catalysis and magnetism.<sup>1</sup>

In the past few decades, various lacunary POMs have been used to capture transition-metal (TM) cations to form novel complexes with interesting structures and properties. Among the family of POMs, TM-substituted polyoxotungstates (POTs) are ideal models for researching magnetic exchange interactions within TM centers. Thus, predominant interest is driven by various electronic and magnetic properties of TM-substituted POTs; to date, numerous TM-substituted POTs have been found,<sup>2</sup> such as [H<sub>56</sub>Fe<sub>28</sub>P<sub>8</sub>W<sub>48</sub>O<sub>248</sub>]<sup>28-</sup> (ref. 2a), [Cu<sub>20</sub>Cl(OH)<sub>24</sub>(H<sub>2</sub>O)<sub>12</sub>(P<sub>8</sub>W<sub>48</sub>O<sub>184</sub>)]<sup>25-</sup> (ref. 2b), [Nb<sub>4</sub>O<sub>6</sub>(Nb<sub>3</sub>-SiW<sub>9</sub>O<sub>40</sub>)<sub>4</sub>]<sup>20-</sup> (ref. 2c), [(P<sub>2</sub>W<sub>15</sub>Ti<sub>3</sub>O<sub>642</sub>)<sub>4</sub>{Ti(OH)<sub>3</sub>Cl}]<sup>45-</sup> (ref. 2d), [Ni(enMe)<sub>2</sub>]<sub>3</sub>[H<sub>8</sub>Ni<sub>20</sub>P<sub>4</sub>W<sub>34</sub>(OH)<sub>4</sub>O<sub>136</sub>(enMe)<sub>8</sub>(H<sub>2</sub>O)<sub>6</sub>·12H<sub>2</sub>O]<sub>2e</sub>, [Ni(en)<sub>2</sub>(H<sub>2</sub>O)]<sub>2</sub>[H<sub>8</sub>Ni<sub>20</sub>P<sub>4</sub>W<sub>34</sub>(OH)<sub>4</sub>O<sub>136</sub>(en)<sub>9</sub>(H<sub>2</sub>O)<sub>4</sub>·16H<sub>2</sub>O]<sub>2e</sub>, [Mn<sub>19</sub>(OH)<sub>12</sub>(SiW<sub>10</sub>O<sub>37</sub>)<sub>6</sub>]<sup>34-</sup> (ref. 2f) and [(Mn<sup>II</sup>(H<sub>2</sub>O)<sub>3</sub>)<sub>2</sub>(K{α-GeW<sub>10</sub>Mn<sup>II</sup>O<sub>38</sub>})]<sup>19-</sup>.<sup>2g</sup> Compared with TM cations, though the larger sizes of lanthanide (Ln) cations prevent them from full incorporation into lacunary POT matrixes, their oxophilicity and high coordination numbers provide available conditions for further deriving complicated structures. Moreover, their functionality such as luminescence,

<sup>a</sup>Institute of Molecular and Crystal Engineering, Henan Key Laboratory of Polyoxometalate Chemistry, College of Chemistry and Chemical Engineering, Henan University, Kaifeng, Henan 475004, P. R. China. E-mail: zhaojunwei@henu.edu.cn

<sup>b</sup>State Key Laboratory of Structural Chemistry, Fujian Institute of Research on the Structure of Matter, Chinese Academy of Sciences, Fuzhou, Fujian 350002, P. R. China. E-mail: ygy@fjirsm.ac.cn

<sup>†</sup>Electronic supplementary information (ESI) available: The refinement details, bond valence sum calculations, additional figures and thermogravimetric analyses. CCDC 967042–967048 for **1–7**. For ESI and crystallographic data in CIF or other electronic format see DOI: 10.1039/c3dt53616e

magnetism or Lewis acid catalysis can be also delivered to the desired outcomes during the course of derivatization or functionality.<sup>3</sup> Therefore, in recent years, a large number of Ln-containing POTs have been obtained.<sup>4</sup> For instance, in 1997, Pope and co-workers reported a Ce<sub>16</sub>-containing huge POT [As<sub>12</sub>Ce<sub>16</sub>W<sub>148</sub>O<sub>524</sub>(H<sub>2</sub>O)<sub>36</sub>]<sup>76-</sup>.<sup>4a</sup> In 2001, a europium containing tetrameric phosphotungstate [(PEuW<sub>10</sub>O<sub>38</sub>)<sub>4</sub>(W<sub>3</sub>O<sub>14</sub>)]<sup>30-</sup> was discovered by Francesconi's group.<sup>4b</sup> In 2002, Gouzerh *et al.* described two cerium-containing POTs [Ce(H<sub>2</sub>O)<sub>5</sub>As<sub>4</sub>W<sub>40</sub>O<sub>140</sub>]<sup>25-</sup> and [(SbW<sub>9</sub>O<sub>33</sub>)<sub>4</sub>(WO<sub>2</sub>(H<sub>2</sub>O))<sub>2</sub>Ce<sub>3</sub>(H<sub>2</sub>O)<sub>8</sub>(Sb<sub>4</sub>O<sub>4</sub>)]<sup>19-</sup>.<sup>4c</sup> In 2003, two crown-shaped europium containing arsenotungstates [KCe{Eu(H<sub>2</sub>O)<sub>2</sub>(α-AsW<sub>9</sub>O<sub>33</sub>)<sub>6</sub>}]<sup>35-</sup> and [CsC{Eu(H<sub>2</sub>O)<sub>2</sub>(α-AsW<sub>9</sub>O<sub>33</sub>)<sub>4</sub>}]<sup>23-</sup> were separated.<sup>4d</sup> In 2007, an unprecedented Ce<sub>20</sub>-containing gigantic germanetungstate (GT) [Ce<sub>20</sub>Ge<sub>10</sub>W<sub>100</sub>O<sub>376</sub>(OH)<sub>4</sub>(H<sub>2</sub>O)<sub>30</sub>]<sup>56-</sup> was prepared.<sup>4e</sup> Later, the longest Ln substituted POT molecule [Gd<sub>8</sub>As<sub>12</sub>W<sub>124</sub>O<sub>432</sub>(H<sub>2</sub>O)<sub>36</sub>]<sup>60-</sup> was discovered.<sup>4f</sup> With the rapid development of POM chemistry, the first POM-based TM–Ln heterometallic derivative (PBTLDH) was reported in 2004.<sup>5</sup> From then on, the design and synthesis of PBTLDHs have gradually become an emerging research field of POM chemistry owing to their potential applications in magnetism and catalysis as well as their intriguing architectures and topologies.<sup>6</sup> However, as previously reported, there are unavoidable competitive reactions among highly negative POM precursors, strongly oxyphilic Ln cations and less active TM cations in the reaction system, so the simultaneous combinations of lacunary POMs with TM and Ln components are comparatively difficult in the same system,<sup>7</sup> which seems to be the key factor of the small number of reports on PBTLDHs.<sup>8</sup> So, currently, great efforts have been devoted to exploitation of novel PBTLDHs and some typical species have been successively synthesized (Fig. 1).<sup>9,6a</sup> Among PBTLDHs, only a minority of TM–Ln-containing GTs have been reported.<sup>10</sup> For example, Reinoso *et al.* prepared two Weakley-type heterometallic Cu/Mn–Ce substituted GTs [{Ce<sup>III</sup>(H<sub>2</sub>O)<sub>2</sub>}<sub>2</sub>Mn<sup>III</sup>(B-α-GeW<sub>9</sub>O<sub>34</sub>)<sub>2</sub>]<sup>8-</sup> (ref. 10a) and [{Ce<sup>IV</sup>(OAc)Cu<sup>II</sup>(H<sub>2</sub>O)(B-α-GeW<sub>9</sub>O<sub>34</sub>)<sub>2</sub>}]<sup>11-</sup> (ref. 10b) by reactions of Ce<sup>IV</sup> cations with the synthons [Mn<sup>II</sup><sub>4</sub>(H<sub>2</sub>O)<sub>2</sub>(B-α-GeW<sub>9</sub>O<sub>34</sub>)<sub>2</sub>]<sup>12-</sup> (ref. 11) and [Cu<sup>II</sup><sub>4</sub>(H<sub>2</sub>O)<sub>2</sub>(B-α-GeW<sub>9</sub>O<sub>34</sub>)<sub>2</sub>]<sup>12-</sup> (ref. 11) in 2010 and 2011, respectively. Furthermore, a giant crown-shaped GT Na<sub>40</sub>K<sub>6</sub>[Ni(H<sub>2</sub>O)<sub>6</sub>]<sub>3</sub>[KCK-Ge<sub>24</sub>Ge<sub>12</sub>W<sub>120</sub>O<sub>456</sub>(OH)<sub>12</sub>(H<sub>2</sub>O)<sub>64</sub>]<sub>178</sub>H<sub>2</sub>O was also obtained by them.<sup>10c</sup> As a result, the search and exploration of novel TM–Ln-containing GTs are still an incipient field. Under this background, we began to explore this challengeable area. Three organic–inorganic hybrid {Cu<sub>3</sub>LnO<sub>4</sub>} cubane inserted GTs {Cu(en)<sub>2</sub>(H<sub>2</sub>O)}[Cu<sub>3</sub>Ln(en)<sub>3</sub>(OH)<sub>3</sub>(H<sub>2</sub>O)<sub>2</sub>](α-GeW<sub>11</sub>O<sub>39</sub>)<sub>2</sub>·*n*H<sub>2</sub>O (Ln = Eu<sup>III</sup>, *n* = 11; Ln = Tb<sup>III</sup>, *n* = 11; Ln = Dy<sup>III</sup>, *n* = 10) and three Cu–Ln-containing GT tetramers Na<sub>2</sub>H<sub>6</sub>[Cu(en)<sub>2</sub>(H<sub>2</sub>O)]<sub>8</sub>{Cu(en)<sub>2</sub>[La(α-GeW<sub>11</sub>O<sub>39</sub>)<sub>2</sub>]}<sub>2</sub>·18H<sub>2</sub>O, K<sub>4</sub>H<sub>2</sub>[Cu(en)<sub>2</sub>(H<sub>2</sub>O)]<sub>5</sub>[Cu(en)<sub>2</sub>(H<sub>2</sub>O)]<sub>2</sub>[Cu(en)<sub>2</sub>]<sub>2</sub>·{Cu(en)<sub>2</sub>[Pr(α-GeW<sub>11</sub>O<sub>39</sub>)<sub>2</sub>]}<sub>2</sub>·16H<sub>2</sub>O and KNa<sub>2</sub>H<sub>7</sub>[enH<sub>2</sub>]<sub>3</sub>{Cu(en)<sub>2</sub>(H<sub>2</sub>O)]<sub>2</sub>[Cu(en)<sub>2</sub>]<sub>2</sub>{Cu(en)<sub>2</sub>[Er(α-GeW<sub>11</sub>O<sub>39</sub>)<sub>2</sub>]}<sub>2</sub>·15H<sub>2</sub>O were first synthesized in our laboratory.<sup>12a</sup> Very recently, we separated two unusual 1-D copper-bridged tetrahedral POM nanoclusters with tetrameric rare earth cores and GT vertexes Na<sub>3</sub>H<sub>7</sub>[Cu(en)<sub>2</sub>]<sub>5</sub>[Cu(en)<sub>2</sub>(H<sub>2</sub>O)]<sub>2</sub>[RE<sub>4</sub>Ge<sub>4</sub>W<sub>46</sub>O<sub>164</sub>(H<sub>2</sub>O)<sub>3</sub>]<sub>*n*</sub>·*n*H<sub>2</sub>O (RE = Gd<sup>III</sup>, *n* = 25; RE = Y<sup>III</sup>, *n* = 23).<sup>12b</sup> In order to profoundly explore this research domain, we used dap (dap = 1,2-diaminopropane) instead of en, and finally, we made a series of novel

organic–inorganic hybrid 1-D double chain GTs [H<sub>2</sub>dap][Cu(dap)<sub>2</sub>]<sub>0.5</sub>[Cu(dap)<sub>2</sub>(H<sub>2</sub>O)][Ln(H<sub>2</sub>O)<sub>3</sub>(α-GeW<sub>11</sub>O<sub>39</sub>)]<sub>2</sub>·3H<sub>2</sub>O [Ln = La<sup>III</sup> (1), Pr<sup>III</sup> (2), Nd<sup>III</sup> (3), Sm<sup>III</sup> (4), Eu<sup>III</sup> (5), Tb<sup>III</sup> (6), Er<sup>III</sup> (7)], which are constituted by two 1-D antiparallel {[Cu(dap)<sub>2</sub>(H<sub>2</sub>O)]-[Ln(H<sub>2</sub>O)<sub>3</sub>(α-GeW<sub>11</sub>O<sub>39</sub>)]<sub>*n*</sub>}<sup>3*n*-</sup> polymeric chains *via* [Cu(dap)<sub>2</sub>]<sup>2+</sup> bridges. The variable-temperature magnetic susceptibilities of 2, 4 and 7 have been measured. Furthermore, the solid-state electrochemical and electro-catalytic properties of 3 and 4 have been measured in 0.5 mol<sup>-1</sup> Na<sub>2</sub>SO<sub>4</sub> + H<sub>2</sub>SO<sub>4</sub> aqueous solution by entrapping them in a carbon paste electrode (CPE). 3- and 4-CPEs were employed to electro-catalyze the reduction of nitrite, bromate and hydrogen peroxide. The results indicate that 3- and 4-CPE exhibit obvious electro-catalytic activities towards the reduction of nitrite, bromate and hydrogen peroxide.

## Experimental

### Materials and physical measurements

All chemicals were commercially purchased and used without further purification. K<sub>8</sub>Na<sub>2</sub>[A-α-GeW<sub>9</sub>O<sub>34</sub>]<sub>2</sub>·25H<sub>2</sub>O was synthesized according to the literature<sup>13</sup> and characterized by IR spectra. Elemental analyses (C, H and N) were performed on a Perkin-Elmer 2400-II CHNS/O analyzer. Inductively coupled plasma atomic emission spectrometry (ICP-AES) was performed on a Perkin-Elmer Optima 2000 ICP-AES spectrometer. Powder X-ray diffraction (PXRD) spectra were performed on a Bruker D8 ADVANCE instrument with Cu Kα radiation (λ = 1.54056 Å). IR spectra were obtained from solid samples palletized with KBr on a Nicolet 170 SXFT-IR spectrometer in the range 400–4000 cm<sup>-1</sup>. TGA were performed under a N<sub>2</sub> atmosphere on a Mettler–Toledo TGA/SDTA 851<sup>e</sup> instrument with a heating rate of 10 °C min<sup>-1</sup> from 25 to 700 °C. XPS spectra were recorded on an Axis Ultra X-ray photoelectron spectrometer and XPS analyses were corrected with reference to C<sub>1s</sub> (284.6 eV). Magnetic measurements were carried out with a Quantum Design MPMS XL-7 magnetometer in the temperature range of 2–300 K. The magnetic susceptibility data were corrected from the diamagnetic contributions as deduced by using Pascal's constant tables. Cyclic voltammograms were recorded on a CS electrochemical workstation (Wuhan Corrtest Instrument Co. Ltd) at room temperature. A conventional three-electrode system was used. Platinum gauze was used as a counter electrode, and an Ag/AgCl electrode was referenced. Chemically bulk-modified carbon paste electrodes (CPEs) were used as working electrodes.

### Preparations of 1–7

[H<sub>2</sub>dap][Cu(dap)<sub>2</sub>(H<sub>2</sub>O)][Cu(dap)<sub>2</sub>]<sub>0.5</sub>[La(H<sub>2</sub>O)<sub>3</sub>(α-GeW<sub>11</sub>O<sub>39</sub>)]<sub>2</sub>·3H<sub>2</sub>O (1). A mixture of K<sub>8</sub>Na<sub>2</sub>[A-α-GeW<sub>9</sub>O<sub>34</sub>]<sub>2</sub>·25H<sub>2</sub>O (0.304 g, 0.099 mmol), CuCl<sub>2</sub>·2H<sub>2</sub>O (0.083 g, 0.487 mmol), LaCl<sub>3</sub> (0.098 g, 0.399 mmol), dap (0.10 mL, 1.201 mmol) and H<sub>2</sub>O (5 mL, 278 mmol) was stirred for 2 h, sealed in a 25 mL Teflon-lined steel autoclave, kept at 160 °C for 5 d and then

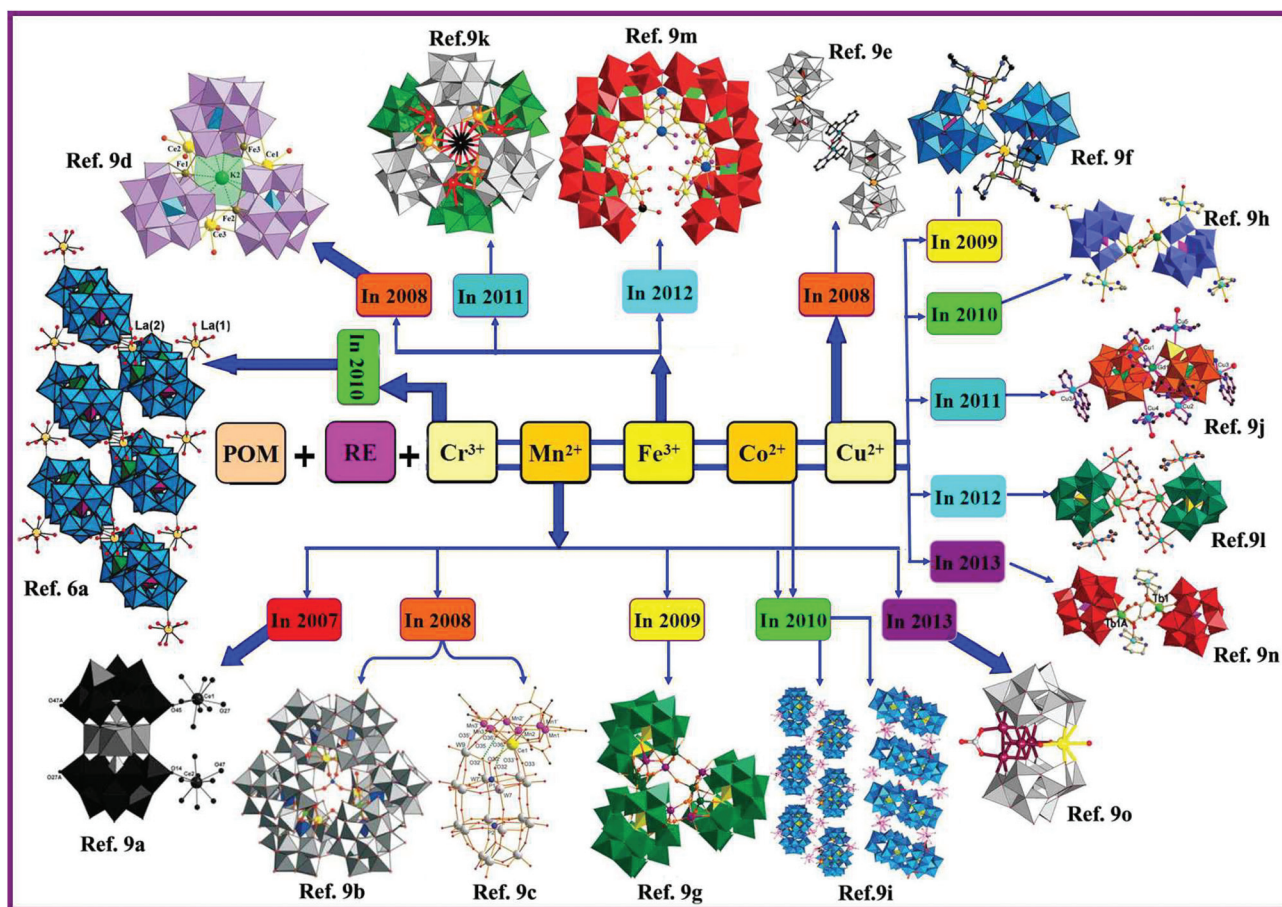


Fig. 1 A summary of some typical 3d–4f POTs.

cooled to room temperature. Purple prismatic crystals were obtained by filtering, washed with distilled water and then dried in air at ambient temperature. Yield: *ca.* 30% (based on  $K_8Na_2[A-\alpha-GeW_9O_{34}]\cdot 25H_2O$ ). Anal. calcd (found %) for  $C_{12}H_{56}Cu_{1.50}GeN_8O_{46}LaW_{11}$  (1): C 4.27 (4.39), H 1.67 (1.82), N 3.32 (3.17), Cu 2.82 (2.72), Ge 2.15 (2.30), La 4.11 (4.32), W 59.87 (59.94). IR (KBr pellets,  $cm^{-1}$ ): 3461(vs), 3306(w), 3253(w), 3139(w), 2968(w), 2928 (w), 1621(m), 1587(m), 1461(w), 1384(w), 1168(w), 1062(m), 1020 (m), 940(s), 873(vs), 811(vs), 767(vs), 692(s) (Fig. S1A and S1B†).

$[H_2dap][Cu(dap)_2(H_2O)][Cu(dap)_2]_{0.5}[Pr(H_2O)_3(\alpha-GeW_{11}O_{39})]\cdot 3H_2O$  (2). A mixture of  $K_8Na_2[A-\alpha-GeW_9O_{34}]\cdot 25H_2O$  (0.366 g, 0.119 mmol),  $CuCl_2\cdot 2H_2O$  (0.109 g, 0.639 mmol),  $PrCl_3$  (0.083 g, 0.336 mmol), *dap* (0.10 mL, 1.201 mmol) and  $H_2O$  (5 mL, 278 mmol) was stirred for 2 h, sealed in a 25 mL Teflon-lined steel autoclave, kept at 160 °C for 5 d and then cooled to room temperature. Purple prismatic crystals were obtained by filtering, washed with distilled water and then dried in air at ambient temperature. Yield: *ca.* 26% (based on  $K_8Na_2[A-\alpha-GeW_9O_{34}]\cdot 25H_2O$ ). Anal. calcd (found %) for  $C_{12}H_{56}Cu_{1.50}GeN_8O_{46}PrW_{11}$ : C 4.26 (4.37), H 1.67 (1.77), N 3.32 (3.44), Cu 2.82 (2.95), Ge 2.15 (2.03), Pr 4.17 (4.04), W 59.83 (59.96). IR (KBr pellets,  $cm^{-1}$ ): 3465(vs), 3307(w), 3248(w),

3142(w), 2969(w), 2928(w), 1617(m), 1589(m), 1468(w), 1386(w), 1167(w), 1056(m), 1023(m), 940(s), 876(vs), 813(vs), 764(vs), 687(s) (Fig. S1A and S1B†).

$[H_2dap][Cu(dap)_2(H_2O)][Cu(dap)_2]_{0.5}[Nd(H_2O)_3(\alpha-GeW_{11}O_{39})]\cdot 3H_2O$  (3). A mixture of  $K_8Na_2[A-\alpha-GeW_9O_{34}]\cdot 25H_2O$  (0.362 g, 0.118 mmol),  $CuCl_2\cdot 2H_2O$  (0.088 g, 0.516 mmol),  $NdCl_3$  (0.095 g, 0.379 mmol), *dap* (0.10 mL, 1.201 mmol) and  $H_2O$  (5 mL, 278 mmol) was stirred for 2 h, sealed in a 25 mL Teflon-lined steel autoclave, kept at 160 °C for 5 d and then cooled to room temperature. Purple prismatic crystals were obtained by filtering, washed with distilled water and then dried in air at ambient temperature. Yield: *ca.* 32% (based on  $K_8Na_2[A-\alpha-GeW_9O_{34}]\cdot 25H_2O$ ). Anal. calcd (found %) for  $C_{12}H_{56}Cu_{1.50}GeN_8O_{46}NdW_{11}$  (3): C 4.26 (4.35), H 1.67 (1.79), N 3.31 (3.20), Cu 2.82 (2.74), Nd 4.26 (4.42), Ge 2.15 (2.09), W 59.78 (59.67). IR (KBr pellets,  $cm^{-1}$ ): 3470(vs), 3302(w), 3251(w), 3140(w), 2971(w), 2932(w), 1619(m), 1588(m), 1462(w), 1397(w), 1168(w), 1064 (m), 1020(m), 941(s), 876(vs), 813(vs), 767(vs), 695(s) (Fig. S1A and S1B†).

$[H_2dap][Cu(dap)_2(H_2O)][Cu(dap)_2]_{0.5}[Sm(H_2O)_3(\alpha-GeW_{11}O_{39})]\cdot 3H_2O$  (4). A mixture of  $K_8Na_2[A-\alpha-GeW_9O_{34}]\cdot 25H_2O$  (0.308 g, 0.100 mmol),  $CuCl_2\cdot 2H_2O$  (0.086 g, 0.504 mmol),  $SmCl_3$  (0.084 g, 0.327 mmol), *dap* (0.10 mL, 1.201 mmol) and  $H_2O$



(5 mL, 278 mmol) was stirred for 2 h, sealed in a 25 mL Teflon-lined steel autoclave, kept at 160 °C for 5 d and then cooled to room temperature. Purple prismatic crystals were obtained by filtering, washed with distilled water and then dried in air at ambient temperature. Yield: *ca.* 35% (based on  $K_8Na_2[A-\alpha-GeW_9O_{34}]\cdot 25H_2O$ ). Anal. calcd (found %) for  $C_{12}H_{56}Cu_{1.50}GeN_8O_{46}SmW_{11}$  (4): C 4.25 (4.11), H 1.67 (1.79), N 3.31 (3.18), Cu 2.81 (2.76), Ge 2.14 (2.25), Sm 4.44 (4.35), W 59.67 (59.50). IR (KBr pellets,  $cm^{-1}$ ): 3468(vs), 3306(w), 3253(w), 3140(w), 2969(w), 2930(w), 1630(m), 1589(m), 1458(w), 1398(w), 1168(w), 1064(m), 1020(m), 941(s), 876(vs), 814(vs), 769(vs), 695(s) (Fig. S1A and S1B†).

$[H_2dap][Cu(dap)_2(H_2O)][Cu(dap)_2]_{0.5}[Eu(H_2O)_3(\alpha-GeW_{11}O_{39})\cdot 3H_2O$  (5). A mixture of  $K_8Na_2[A-\alpha-GeW_9O_{34}]\cdot 25H_2O$  (0.302 g, 0.098 mmol),  $CuCl_2\cdot 2H_2O$  (0.098 g, 0.575 mmol),  $EuCl_3$  (0.089 g, 0.345 mmol), dap (0.10 mL, 1.201 mmol) and  $H_2O$  (5 mL, 278 mmol) was stirred for 2 h, sealed in a 25 mL Teflon-lined steel autoclave, kept at 160 °C for 5 d and then cooled to room temperature. Purple prismatic crystals were obtained by filtering, washed with distilled water and then dried in air at ambient temperature. Yield: *ca.* 33% (based on  $K_8Na_2[A-\alpha-GeW_9O_{34}]\cdot 25H_2O$ ). Anal. calcd (found %) for  $C_{12}H_{56}Cu_{1.50}GeN_8O_{46}EuW_{11}$  (5): C 4.25 (4.36), H 1.66 (1.88), N 3.30 (3.17), Cu 2.81 (2.68), Ge 2.14 (2.01), Eu 4.48 (4.66), W 59.64 (59.83). IR (KBr pellets,  $cm^{-1}$ ): 3467(vs), 3306(w), 3252(w), 3140(w), 2964(w), 2928(w), 1620(m), 1588(m), 1461(w), 13917(w), 1175(w), 1065(m), 1020(m), 942(s), 875(vs), 810(vs), 766(vs), 693(s) (Fig. S1A and S1B†).

$[H_2dap][Cu(dap)_2(H_2O)][Cu(dap)_2]_{0.5}[Tb(H_2O)_3(\alpha-GeW_{11}O_{39})\cdot 3H_2O$  (6). A mixture of  $K_8Na_2[A-\alpha-GeW_9O_{34}]\cdot 25H_2O$  (0.287 g, 0.093 mmol),  $CuCl_2\cdot 2H_2O$  (0.065 g, 0.381 mmol),  $TbCl_3$  (0.086 g, 0.324 mmol), dap (0.10 mL, 1.201 mmol) and  $H_2O$  (5 mL, 278 mmol) was stirred for 2 h, sealed in a 25 mL Teflon-lined steel autoclave, kept at 160 °C for 5 d and then cooled to room temperature. Purple prismatic crystals were obtained by filtering, washed with distilled water and then dried in air at ambient temperature. Yield: *ca.* 33% (based on  $K_8Na_2[A-\alpha-GeW_9O_{34}]\cdot 25H_2O$ ). Anal. calcd (found %) for  $C_{12}H_{56}Cu_{1.50}GeN_8O_{46}TbW_{11}$  (6): C 4.24 (4.17), H 1.66 (1.79), N 3.30 (3.48), Cu 2.80 (2.91), Ge 2.14 (2.30), Tb 4.68 (4.56), W 59.52 (59.61). IR (KBr pellets,  $cm^{-1}$ ): 3477(vs), 3308(w), 3255(w), 3143(w), 2970(w), 2931(w), 1619(m), 1588(m), 1460(w), 1398(w), 1165(w), 1064(m), 1020(m), 943(s), 877(vs), 813(vs), 768(vs), 697(s) (Fig. S1A and S1B†).

$[H_2dap][Cu(dap)_2(H_2O)][Cu(dap)_2]_{0.5}[Er(H_2O)_3(\alpha-GeW_{11}O_{39})\cdot 3H_2O$  (7). A mixture of  $K_8Na_2[A-\alpha-GeW_9O_{34}]\cdot 25H_2O$  (0.307 g, 0.099 mmol),  $CuCl_2\cdot 2H_2O$  (0.098 g, 0.575 mmol),  $ErCl_3$  (0.107 g, 0.391 mmol), dap (0.10 mL, 1.201 mmol) and  $H_2O$  (5 mL, 278 mmol) was stirred for 2 h, sealed in a 25 mL Teflon-lined steel autoclave, kept at 160 °C for 5 d and then cooled to room temperature. Purple prismatic crystals were obtained by filtering, washed with distilled water and then dried in air at ambient temperature. Yield: *ca.* 33% (based on  $K_8Na_2[A-\alpha-GeW_9O_{34}]\cdot 25H_2O$ ). Anal. calcd (found %) for  $C_{12}H_{56}Cu_{1.50}GeN_8O_{46}ErW_{11}$  (7): C 4.23 (4.34), H 1.66 (1.81), N 3.29 (3.14), Cu 2.80 (2.91), Er 4.91 (4.80), Ge 2.13 (2.04),

W 59.37 (59.03). IR (KBr pellets,  $cm^{-1}$ ): 3486(vs), 3307(w), 3258(w), 3143(w), 2970(w), 2930(w), 1620(m), 1587(m), 1461(w), 1384(w), 1175(w), 1065(m), 1019 (m), 944(s), 879(vs), 812(vs), 767(vs), 695(s) (Fig. S1A and S1B†).

### Preparations of 3- and 4-CPE

3-modified CPE (3-CPE) was fabricated as follows: 30 mg of graphite powder and 10 mg of 3 were mixed and ground together by an agate mortar and pestle to achieve a uniform mixture, and then 0.05 mL of paraffin oil was added with stirring. The homogenized mixture was packed into a glass tube with 3.0 mm inner diameter, and the tube surface was wiped with paper. Electrical contact was established with a Cu rod through the back of the electrode. In a similar manner, 4-CPE was made with 4.

### X-ray crystallography

Intensity data for 1–7 were collected on a Bruker APEX-II CCD detector at 296(2) K with Mo  $K\alpha$  radiation ( $\lambda = 0.71073$  Å). Direct methods were used to solve their structures and to locate the heavy atoms using the SHELXTL-97 program package.<sup>14</sup> The remaining non-hydrogen atoms were found from successive difference Fourier syntheses and full-matrix least-squares refinements on  $F^2$ . Lorentz polarization and empirical absorption corrections were applied. No hydrogen atoms associated with water molecules were located from the difference Fourier map. The positions of hydrogen atoms attached to carbon and nitrogen atoms were geometrically placed. All hydrogen atoms were refined isotropically as a riding model using the default SHELXTL parameters. All the non-hydrogen atoms were anisotropically refined except for some water molecules, oxygen, carbon and nitrogen atoms (details are seen in ESI†). Crystallographic data and structure refinements for 1–7 are summarized in Table 1. Crystallographic data for the structures reported in this paper have been deposited in the Cambridge Crystallographic Data Centre with CCDC 967043, 967044, 967042, 967045, 967046, 967047 and 967048 for 1, 2, 3, 4, 5, 6 and 7, respectively.

## Results and discussion

### Syntheses

1–7 were obtained from the reaction of lacunary GT precursor  $[\alpha-A-GeW_9O_{34}]^{10-}$  with  $Cu^{II}$  and  $Ln^{III}$  cations in the participation of dap under hydrothermally conditions. Though the trivalent Keggin  $[\alpha-A-GeW_9O_{34}]^{10-}$  precursor has been intensively exploited since 2004,<sup>11</sup> investigations on the reactions of the  $[\alpha-A-GeW_9O_{34}]^{10-}$  precursor, TM and Ln cations are rare. Considering the advantages of hydrothermal conditions, the flexibility of various coordination modes and the Jahn–Teller effect of  $Cu^{II}$  ions, and the oxophilicity and high coordination numbers of  $Ln^{III}$  cations, the system including  $[\alpha-A-GeW_9O_{34}]^{10-}$ ,  $Cu^{II}$  and  $Ln^{III}$  was developed and some neoteric Cu–Ln containing GTs were made.<sup>12</sup> Three double  $\{Cu_3LnO_4\}$  cubane inserted GTs  $\{[Cu(en)_2(H_2O)][Cu_3Ln-$

Table 1 X-ray diffraction crystallographic data and structure refinements for 1–7

	1	2	3	4	5	6	7
Empirical formula	C <sub>12</sub> H <sub>56</sub> Cu <sub>1.5</sub> Ge- LaN <sub>8</sub> O <sub>46</sub> W <sub>11</sub>	C <sub>12</sub> H <sub>56</sub> Cu <sub>1.50</sub> Ge- PrN <sub>8</sub> O <sub>46</sub> W <sub>11</sub>	C <sub>12</sub> H <sub>56</sub> Cu <sub>1.5</sub> Ge- NdN <sub>8</sub> O <sub>46</sub> W <sub>11</sub>	C <sub>12</sub> H <sub>56</sub> Cu <sub>1.50</sub> - GeSmN <sub>8</sub> O <sub>46</sub> W <sub>11</sub>	C <sub>12</sub> H <sub>56</sub> Cu <sub>1.50</sub> - GeEuN <sub>8</sub> O <sub>46</sub> W <sub>11</sub>	C <sub>12</sub> H <sub>56</sub> Cu <sub>1.50</sub> - GeTbN <sub>8</sub> O <sub>46</sub> W <sub>11</sub>	C <sub>12</sub> H <sub>56</sub> Cu <sub>1.50</sub> Ge- ErN <sub>8</sub> O <sub>46</sub> W <sub>11</sub>
Formula weight	3377.81	3379.73	3383.14	3389.25	3390.86	3397.72	3406.16
Crystal system	Triclinic	Triclinic	Triclinic	Triclinic	Triclinic	Triclinic	Triclinic
Space group	<i>P</i> $\bar{1}$	<i>P</i> $\bar{1}$	<i>P</i> $\bar{1}$	<i>P</i> $\bar{1}$	<i>P</i> $\bar{1}$	<i>P</i> $\bar{1}$	<i>P</i> $\bar{1}$
<i>a</i> (Å)	11.5054(11)	11.430(2)	11.4615(14)	11.408(3)	11.327(6)	11.472(5)	11.2900(8)
<i>b</i> (Å)	12.5391(12)	12.540(3)	12.6091(15)	12.563(4)	12.493(6)	12.626(6)	12.4765(9)
<i>c</i> (Å)	21.400(2)	21.298(4)	21.456(3)	21.400(6)	21.298(10)	21.551(10)	21.3987(15)
$\alpha$ (°)	86.083(2)	85.591(4)	85.706(2)	85.602(5)	85.454(9)	85.036(7)	84.6320(10)
$\beta$ (°)	76.139(2)	76.173(4)	76.120(2)	75.868(5)	75.769(12)	75.206(7)	74.8200(10)
$\gamma$ (°)	74.298(2)	73.999(4)	74.166(2)	74.308(5)	74.292(11)	74.721(7)	75.3590(10)
<i>V</i> (Å <sup>3</sup> )	2885.6(5)	2849.2(10)	2895.9(6)	2863.3(14)	2812(2)	2911(2)	2813.4(3)
<i>Z</i>	2	2	2	2	2	2	2
$\mu$ (mm <sup>-1</sup> )	23.702	24.110	23.776	24.166	24.679	23.980	25.043
<i>F</i> (000)	2997	3000	3003	3007	3009	3033	3019
<i>T</i> (K)	296(2)	296(2)	296(2)	296(2)	296(2)	296(2)	296(2)
Limiting indices	-13 ≤ <i>h</i> ≤ 13 -14 ≤ <i>k</i> ≤ 14 -24 ≤ <i>l</i> ≤ 25	-12 ≤ <i>h</i> ≤ 13 -14 ≤ <i>k</i> ≤ 14 -25 ≤ <i>l</i> ≤ 24	-13 ≤ <i>h</i> ≤ 13 -14 ≤ <i>k</i> ≤ 14 -18 ≤ <i>l</i> ≤ 25	-13 ≤ <i>h</i> ≤ 13 -14 ≤ <i>k</i> ≤ 14 -17 ≤ <i>l</i> ≤ 25	-10 ≤ <i>h</i> ≤ 13 -13 ≤ <i>k</i> ≤ 14 -24 ≤ <i>l</i> ≤ 25	-13 ≤ <i>h</i> ≤ 13 -15 ≤ <i>k</i> ≤ 14 -21 ≤ <i>l</i> ≤ 25	-13 ≤ <i>h</i> ≤ 12 -14 ≤ <i>k</i> ≤ 14 -22 ≤ <i>l</i> ≤ 25
No. of reflections collected	14 704	14 412	14 273	14 149	14 237	14 707	14 387
No. of independent reflections	10 036	9919	9943	9897	9798	10 105	9717
<i>R</i> <sub>int</sub>	0.0534	0.0316	0.0590	0.0922	0.1504	0.0532	0.1150
Data/restraints/parameters	10 036/170/657	9919/25/672	9943/86/672	9897/149/632	9798/208/587	10 105/11/658	9717/89/658
GOFO <i>F</i> <sup>2</sup>	0.990	1.016	1.034	1.005	0.997	1.032	1.000
Final <i>R</i> indices	<sup>a</sup> <i>R</i> <sub>1</sub> = 0.0622	<i>R</i> <sub>1</sub> = 0.0477	<i>R</i> <sub>1</sub> = 0.0735	<i>R</i> <sub>1</sub> = 0.0964	<i>R</i> <sub>1</sub> = 0.1131	<i>R</i> <sub>1</sub> = 0.0614	<i>R</i> <sub>1</sub> = 0.0637
[ <i>I</i> > 2σ( <i>I</i> )]	<sup>b</sup> w <i>R</i> <sub>2</sub> = 0.1600	w <i>R</i> <sub>2</sub> = 0.1143	w <i>R</i> <sub>2</sub> = 0.1858	w <i>R</i> <sub>2</sub> = 0.2208	w <i>R</i> <sub>2</sub> = 0.1712	w <i>R</i> <sub>2</sub> = 0.1594	w <i>R</i> <sub>2</sub> = 0.1801
<i>R</i> indices (all data)	<i>R</i> <sub>1</sub> = 0.0815	<i>R</i> <sub>1</sub> = 0.0705	<i>R</i> <sub>1</sub> = 0.0896	<i>R</i> <sub>1</sub> = 0.1474	<i>R</i> <sub>1</sub> = 0.2430	<i>R</i> <sub>1</sub> = 0.0731	<i>R</i> <sub>1</sub> = 0.0715
	w <i>R</i> <sub>2</sub> = 0.1726	w <i>R</i> <sub>2</sub> = 0.1220	w <i>R</i> <sub>2</sub> = 0.1956	w <i>R</i> <sub>2</sub> = 0.2491	w <i>R</i> <sub>2</sub> = 0.1969	w <i>R</i> <sub>2</sub> = 0.1675	w <i>R</i> <sub>2</sub> = 0.1866
Largest diff. peak and hole, e Å <sup>-3</sup>	3.588, -3.868	2.551, -3.169	4.429, -5.716	4.273, -4.501	3.422, -4.412	3.799, -4.266	4.486, -4.381

<sup>a</sup> *R*<sub>1</sub> =  $\sum ||F_o| - |F_c|| / \sum |F_o|$ . <sup>b</sup> w*R*<sub>2</sub> =  $[\sum w(F_o^2 - F_c^2)^2 / \sum w(F_o^2)^2]^{1/2}$ ; w =  $1/[\sigma^2(F_o^2) + (xP)^2 + yP]$ ; *P* =  $(F_o^2 + 2F_c^2)/3$ , where *x* = 0.0999, *y* = 0.0000 for 1; *x* = 0.0601, *y* = 0.0000 for 2; *x* = 0.1070, *y* = 0.0000 for 3; *x* = 0.0368, *y* = 0.0000 for 4; *x* = 0.0267, *y* = 0.0000 for 5; *x* = 0.0958, *y* = 0.0000 for 6; *x* = 0.1413, *y* = 0.0000 for 7.

(en)<sub>3</sub>(OH)<sub>3</sub>(H<sub>2</sub>O)<sub>2</sub>[(α-GeW<sub>11</sub>O<sub>39</sub>)<sub>2</sub>]<sub>2</sub>·*n*H<sub>2</sub>O (Ln = Eu<sup>III</sup>, *n* = 11; Ln = Tb<sup>III</sup>, *n* = 11; Ln = Dy<sup>III</sup>, *n* = 10) and three tetrameric architectures {Cu(en)<sub>2</sub>[Ln(α-GeW<sub>11</sub>O<sub>39</sub>)<sub>2</sub>]<sub>2</sub>}<sup>24-</sup> (Ln = La<sup>III</sup>, Pr<sup>III</sup>, Er<sup>III</sup>) built by two 1:2-type [Ln(α-GeW<sub>11</sub>O<sub>39</sub>)<sub>2</sub>]<sup>13-</sup> moieties *via* a [Cu(en)<sub>2</sub>]<sup>2+</sup> bridge were first obtained.<sup>12a</sup> When Gd<sup>III</sup> or Y<sup>III</sup> cations were introduced to the system, two tetrahedral PBTLDH nanoclusters Na<sub>3</sub>H<sub>7</sub>[Cu(en)<sub>2</sub>]<sub>5</sub>[Cu(en)<sub>2</sub>(H<sub>2</sub>O)]<sub>2</sub>[RE<sub>4</sub>Ge<sub>4</sub>W<sub>46</sub>O<sub>164</sub>(H<sub>2</sub>O)<sub>3</sub>]<sub>2</sub>·*n*H<sub>2</sub>O (RE = Gd<sup>III</sup>, *n* = 25; RE = Y<sup>III</sup>, *n* = 23) were synthesized.<sup>12b</sup> As ongoing efforts in this branch, when dap replaced en, seven isomorphous Cu<sup>II</sup>-Ln<sup>III</sup> containing GTs 1–7 were sequentially separated, whose main skeletons are constructed from the 1-D Cu<sup>II</sup>-Ln<sup>III</sup> heterometallic GT double-chains by means of the bridging role of [Cu(dap)<sub>2</sub>]<sup>2+</sup> cations. From the above results, several points can be mentioned here: (a) All Cu<sup>II</sup>-Ln<sup>III</sup> containing GTs prepared by us consist of [α-GeW<sub>11</sub>O<sub>39</sub>]<sup>8-</sup> fragments although we used the [α-A-GeW<sub>9</sub>O<sub>34</sub>]<sup>10-</sup> precursor, indicating that it is favorable for conversion from [α-A-GeW<sub>9</sub>O<sub>34</sub>]<sup>10-</sup> to [α-GeW<sub>11</sub>O<sub>39</sub>]<sup>8-</sup> during the course of formation. When K<sub>6</sub>Na<sub>2</sub>[α-GeW<sub>11</sub>O<sub>39</sub>]<sub>2</sub>·13H<sub>2</sub>O replaced K<sub>8</sub>Na<sub>2</sub>[α-A-GeW<sub>9</sub>O<sub>34</sub>]<sub>2</sub>·25H<sub>2</sub>O under similar conditions, the same target products cannot be afforded, which can further support this proposal. (b) Organic ligands have an important influence on the structural construction of the

outcomes. When dap replaced en, we obtained 1-D double-chain Cu<sup>II</sup>-Ln<sup>III</sup> heterometallic GTs reported in this paper. (c) The nature of Ln<sup>III</sup> ions greatly affects structural constructions in the [α-A-GeW<sub>9</sub>O<sub>34</sub>]<sup>10-</sup>, Cu<sup>II</sup>, Ln<sup>III</sup> and en system whereas the nature of Ln<sup>III</sup> ions has no obvious effect on structural constructions in the [α-A-GeW<sub>9</sub>O<sub>34</sub>]<sup>10-</sup>, Cu<sup>II</sup>, Ln<sup>III</sup> and dap system. For example, in the presence of en, double {Cu<sub>3</sub>LnO<sub>4</sub>} cubane inserted GTs were made for Eu<sup>III</sup>, Tb<sup>III</sup> and Dy<sup>III</sup> cations, tetrameric {Cu(en)<sub>2</sub>[Ln(α-GeW<sub>11</sub>O<sub>39</sub>)<sub>2</sub>]<sub>2</sub>}<sup>24-</sup> were formed for La<sup>III</sup>, Pr<sup>III</sup> and Er<sup>III</sup> cations while copper-bridged tetrahedral PBTLDH nanoclusters are only formed by virtue of Gd<sup>III</sup> or Y<sup>III</sup> cations. In the participation of dap, only 1-D double-chain Cu<sup>II</sup>-Ln<sup>III</sup> heterometallic GTs were obtained. (d) The nature of TM cations can also influence the structural diversity of the products. Ni<sup>II</sup> or Co<sup>II</sup> were used in the presence of Ln<sup>III</sup> ions under similar conditions; unfortunately, only organic-inorganic hybrid TM substituted GTs [enH<sub>2</sub>]<sub>2</sub>[Ni(en)<sub>2</sub>]<sub>2</sub>·{[Ni<sub>6</sub>(en)<sub>2</sub>(H<sub>2</sub>O)<sub>2</sub>][B-α-GeW<sub>9</sub>O<sub>34</sub>]<sub>2</sub>}·14H<sub>2</sub>O<sup>15a</sup> and {[Co(dap)<sub>2</sub>(H<sub>2</sub>O)<sub>2</sub>][Co(dap)<sub>2</sub>][Co<sub>4</sub>(Hdap)<sub>2</sub>(B-α-HGeW<sub>9</sub>O<sub>34</sub>)<sub>2</sub>]}·7H<sub>2</sub>O<sup>15b</sup> were obtained. When other TM ions such as Ti<sup>4+</sup>, Cr<sup>3+</sup>, Fe<sup>2+</sup> and Cd<sup>2+</sup> ions were used, however, amorphous powders were obtained. In the future, we will introduce other functional organic ligands such as aliphatic polycarboxylic acid and

aromatic polycarboxylic acid ligands to the system to prepare much more TM–Ln containing GTs with excellent properties and novel architectures.

### Structural descriptions

Bond valence sum (BVS) calculations<sup>17a–c</sup> of **1–7** indicate that the oxidation states of all W, Cu and Ln atoms are +6, +2 and +3, respectively (Table S1†) and **1**, **3**, **5** and **7** are further confirmed by XPS spectra (Fig. 2 and S2†). The W4f<sub>7/2</sub> and W4f<sub>5/2</sub> binding energies of 34.0 and 35.7 eV for **1**, 33.5 and 35.6 eV for **3**, 34.0 and 35.9 eV for **5**, 33.8 and 35.9 eV for **7** are coincident with the previous results,<sup>18a–c</sup> which indicate that all the W centers are +6 in **1**, **3**, **5**, **7**. The spin–orbit components (2p<sub>3/2</sub> and 2p<sub>1/2</sub>) of the Cu2p peak are well deconvoluted by two curves at 932.9 and 952.6 eV for **1**, 932.8 and 952.0 eV for **3**, 932.8 and 953.2 eV for **5**, 933.3 and 953.0 eV for **7**. These values are in line with the reported values,<sup>18d</sup> confirming the presence of the Cu<sup>II</sup> cations in **1**, **3**, **5** and **7**. Two peaks at 833.4 and 853.6 eV correspond to the La3d<sub>5/2</sub> and La3d<sub>3/2</sub> of the La<sup>III</sup> cation in **1**.<sup>18e</sup> The peaks at 979.9 and 1003.7 eV are ascribed to the Nd3d<sub>5/2</sub> and Nd3d<sub>3/2</sub> of the Nd<sup>III</sup> cation in **3**.<sup>18f</sup> In **5**, the XPS profile exhibits two peaks at 1132.3 and 1162.0 eV, which are assigned to the 3d<sub>5/2</sub> and 3d<sub>3/2</sub> levels of the Eu<sup>III</sup> cation.<sup>18g</sup> The Er<sup>III</sup>4d<sub>3/2</sub> peak is found at 170.4 eV.<sup>18f</sup> These results are consistent with BVS calculations from the X-ray structural analysis data.

The phase purity of **1–7** is supported by the agreement of the PXRD patterns of the bulks with the calculated patterns from the single-crystal structural analyses (Fig. S3 and S4†). The intensity differences between experimental and simulated PXRD patterns are due to the variation in preferred orientation of the powder sample during collection of the experimental PXRD. Single-crystal X-ray structural analyses display that **1–7** are isomorphous and all crystallize in the triclinic space group *P* $\bar{1}$ . **1–7** all display a 1-D double-chain architecture formed by two 1-D antiparallel Cu<sup>II</sup>–Ln<sup>III</sup> heterometallic GT polymeric chains  $\{[\text{Cu}(\text{dap})_2(\text{H}_2\text{O})][\text{Ln}(\text{H}_2\text{O})_3(\alpha\text{-GeW}_{11}\text{O}_{39})]\}_n^{3n-}$  by means of the bridging functionality of the  $[\text{Cu}(\text{dap})_2]^{2+}$  cations. Herein, only the structure of **1** is described in detail. Additionally, because of the existence of the Jahn–Teller effect of Cu<sup>II</sup> ions in the ligand field resulting in the elongation of the Cu–O distances, the Cu–O weak interactions will be considered in the following description. The asymmetrical structural unit  $[\text{H}_2\text{dap}][\text{Cu}(\text{dap})_2]_{0.5}[\text{Cu}(\text{dap})_2(\text{H}_2\text{O})][\text{Ln}(\text{H}_2\text{O})_3(\alpha\text{-GeW}_{11}\text{O}_{39})] \cdot 3\text{H}_2\text{O}$  of **1** (Fig. 3a) consists of a mono-La<sup>III</sup> substituted Keggin-type  $[\text{Ln}(\text{H}_2\text{O})_3(\alpha\text{-GeW}_{11}\text{O}_{39})]^{5-}$  subunit, half  $[\text{Cu}(\text{dap})_2]^{2+}$  bridging cation, one pendent  $[\text{Cu}(\text{dap})_2(\text{H}_2\text{O})]^{2+}$  cation, a diprotonated  $[\text{H}_2\text{dap}]^{2+}$  and three lattice water molecules. In the asymmetrical structural unit, the pendent  $[\text{Cu}(\text{dap})_2(\text{H}_2\text{O})]^{2+}$  cation links to the  $[\text{Ln}(\text{H}_2\text{O})_3(\alpha\text{-GeW}_{11}\text{O}_{39})]^{5-}$  subunit *via* a terminal oxygen atom and is embedded in a severely distorted octahedral geometry, in which four nitrogen atoms from two dap ligands occupy the basal plane [Cu–N: 1.993(19)–2.022(18) Å] and a terminal oxygen atom [Cu–O: 3.277(11) Å] and a water ligand [Cu–O: 2.321(16) Å] stand on two axial positions. The bridging  $[\text{Cu}(\text{dap})_2]^{2+}$  cation is located on the special site with

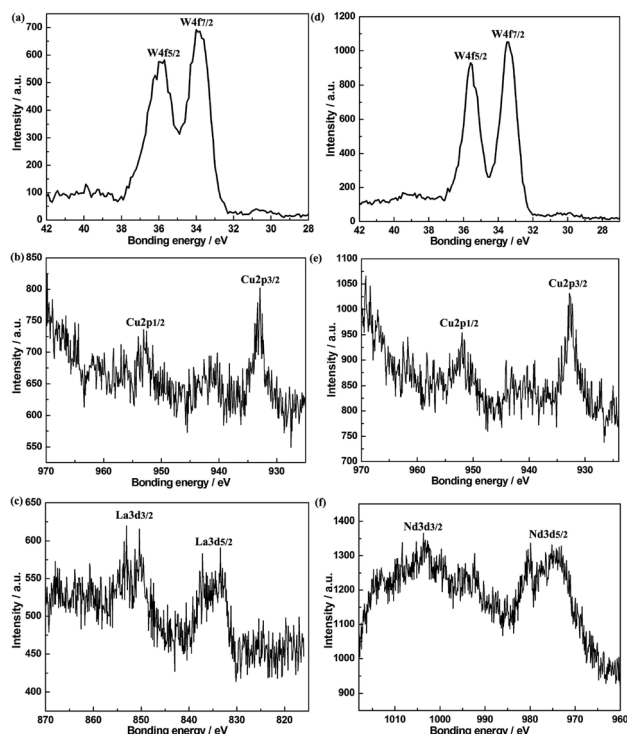


**Fig. 2** (a) The XPS spectrum for W4f<sub>7/2</sub> and W4f<sub>5/2</sub> in **1**; (b) the XPS spectrum for Cu2p<sub>3/2</sub> and Cu2p<sub>1/2</sub> in **1**; (c) the XPS spectrum for La3d<sub>5/2</sub> and La3d<sub>3/2</sub> in **1**; (d) the XPS spectrum for W4f<sub>7/2</sub> and W4f<sub>5/2</sub> in **3**; (e) the XPS spectrum for Cu2p<sub>3/2</sub> and Cu2p<sub>1/2</sub> in **3**; and (f) the XPS spectrum for Nd3d<sub>5/2</sub> and Nd3d<sub>3/2</sub> in **3**.

the atomic coordinate (0.5, 0.5, 0) leading to an occupancy of 50% and inhabits an elongated octahedron defined by four nitrogen atoms from two dap ligands with Cu–N distances of 1.97(3)–1.99(3) Å building the equatorial plane and two oxygen atoms from two adjacent  $[\text{Ln}(\text{H}_2\text{O})_3(\alpha\text{-GeW}_{11}\text{O}_{39})]^{5-}$  subunits with long Cu–O distances of 3.310(42) Å occupying two polar sites. The  $[\text{Cu}(\text{dap})_2(\text{H}_2\text{O})]^{2+}$  and  $[\text{Cu}(\text{dap})_2]^{2+}$  cations display elongated octahedral geometries, proving the occurrence of Jahn–Teller distortion of the copper cations in the ligand field,<sup>19</sup> from which it can be inferred that both Cu1 and Cu2 cations adopt the electron configuration of  $(t_{2g})^6(d_{x^2-y^2})^1(d_{z^2})^2$ . The La<sup>III</sup> cation is captured by the monovacant distorted square antiprismatic geometry (Fig. 3b). The La<sup>III</sup> cation is coordinated by eight oxygen atoms, four of which come from one  $[\alpha\text{-GeW}_{11}\text{O}_{39}]^{8-}$  fragment [La–O: 2.428(14)–2.488(13) Å], and one from the other neighboring  $[\alpha\text{-GeW}_{11}\text{O}_{39}]^{8-}$  fragment [La–O: 2.526(15) Å]. In the coordinate polyhedron around the La<sup>III</sup> cation, the O7, O2W, O3W and O4W group and the O30, O33, O35 and O39 group constitute two bottom planes of the square antiprism and the average deviations from their ideal planes are 0.1012 and 0.0072 Å, respectively. The distances between the La cation and two bottom planes are 1.4911 and 1.1312 Å, respectively. Especially, the La–O7 distance of 2.526(15) Å is much longer than those of the other La–O bond (La–O30, La–O33, La–O35,



La-O39) distances because the W-O-La-O7-W linkage participates in the construction of the 1-D chain (Fig. 4a). More interesting is that two asymmetrical structural units of **1** are joined together by means of the  $[\text{Cu}_2(\text{dap})_2]^{2+}$  cation constructing the dimeric structural unit  $\{[\text{Cu}(\text{dap})_2(\text{H}_2\text{O})][\text{La}(\text{H}_2\text{O})_3(\alpha\text{-GeW}_{11}\text{O}_{39})]\}_2^{6-}$  (Fig. 3c). The most remarkable structural characteristic of **1** is that each dimeric structural unit  $\{[\text{Cu}(\text{dap})_2(\text{H}_2\text{O})][\text{La}(\text{H}_2\text{O})_3(\alpha\text{-GeW}_{11}\text{O}_{39})]\}_2^{6-}$  connects two adjacent identical units through four W-O-La-O-W bridges and constructs the beautiful 1-D antiparallel double-chain motif (Fig. 4b). Alternatively, the 1-D antiparallel double-chain structure can be also viewed as a fusion of two 1-D linear chains  $\{[\text{Cu}(\text{dap})_2(\text{H}_2\text{O})][\text{La}(\text{H}_2\text{O})_3(\alpha\text{-GeW}_{11}\text{O}_{39})]\}_n^{3n-}$  formed by asymmetrical structural units  $\{[\text{Cu}(\text{dap})_2(\text{H}_2\text{O})][\text{La}(\text{H}_2\text{O})_3(\alpha\text{-GeW}_{11}\text{O}_{39})]\}_2^{6-}$  via  $[\text{Cu}_2(\text{dap})_2]^{2+}$  linkers (Fig. 4a and 4b). Actually, other 1-D polymeric chains created by mono-Ln substituted Keggin moieties have been previously observed. For example, in 2000, Pope and co-workers communicated two 1-D inorganic zigzag chain-like Ln-containing monovacant Keggin silicotungstates  $[\text{Ln}(\alpha\text{-SiW}_{11}\text{O}_{39})(\text{H}_2\text{O})_3]^{5-}$  (Ln = Ce<sup>III</sup>, La<sup>III</sup>).<sup>20a</sup> In 2003, Mialane *et al.* discovered a 1-D inorganic linear  $[\text{Yb}(\alpha\text{-SiW}_{11}\text{O}_{39})(\text{H}_2\text{O})_2]^{5-}$  chain and a 1-D zigzag  $[\text{Nd}_2(\alpha\text{-SiW}_{11}\text{O}_{39})(\text{H}_2\text{O})_{11}]^{2-}$  chain.<sup>20b</sup> Later, Niu *et al.* reported a 1-D inorganic/organic-inorganic zigzag chain  $\text{K}_3\{[\text{Pr}(\text{H}_2\text{O})_4(\alpha\text{-SiW}_{11}\text{O}_{39})][\text{NaPr}_2(\text{H}_2\text{O})_{12}][\text{Pr}(\text{H}_2\text{O})_4(\alpha\text{-SiW}_{11}\text{O}_{39})]\} \cdot 13\text{H}_2\text{O}$ ,<sup>20c</sup>  $(\text{CH}_3)_4\text{N}\}_2 \cdot 5\text{H}_2\text{O} \cdot 5[\text{Y}(\text{GeW}_{11}\text{O}_{39})(\text{H}_2\text{O})_2] \cdot 4\text{H}_2\text{O}$ ,<sup>20d</sup> and  $\{\text{Dy}(\text{H}_2\text{O})_7[\text{Dy}(\text{H}_2\text{O})_2(\text{DMSO})(\alpha\text{-GeW}_{11}\text{O}_{39})]\}_2^{2-}$ .<sup>20e</sup> To the best of our knowledge, **1-7** are the first organic-inorganic hybrid 1-D double-chain Cu<sup>II</sup>-Ln<sup>III</sup> heterometallic GTs albeit a GT-based Sm<sup>III</sup>-containing 1-D double-chain GT  $[\text{Sm}_2(\alpha\text{-GeW}_{11}\text{O}_{39})(\text{DMSO})_3(\text{H}_2\text{O})_6]^{2-}$  (ref. 20d) and inorganic 1-D Cr<sup>III</sup>-La<sup>III</sup> heterometallic double-chain silicotungstate  $[(\gamma\text{-SiW}_{10}\text{O}_{36})_2(\text{Cr}(\text{OH})(\text{H}_2\text{O}))_3(\text{La}(\text{H}_2\text{O})_7)_2]^{4-}$  (ref. 20f) has been addressed. It should be

mentioned that there are two types of parallelograms in the double-chain structure of **1** (Fig. 5), the violet parallelogram with the side lengths of  $21.9508 \times 11.5054 \text{ \AA}$  and the inner angle of  $146.234(12)^\circ$  is made up of four La<sup>III</sup> cations from two dimeric structural units  $\{[\text{Cu}(\text{dap})_2(\text{H}_2\text{O})][\text{La}(\text{H}_2\text{O})_3(\alpha\text{-GeW}_{11}\text{O}_{39})]\}_2^{6-}$  and the blue parallelogram with the side lengths of  $14.5378 \times 11.5054 \text{ \AA}$  and the inner angle of  $47.532(16)^\circ$  is constituted by four Ge<sup>IV</sup> atoms from two dimeric structural units  $\{[\text{Cu}(\text{dap})_2(\text{H}_2\text{O})][\text{La}(\text{H}_2\text{O})_3(\alpha\text{-GeW}_{11}\text{O}_{39})]\}_2^{6-}$ . The intersection line of two parallelograms passes through two Cu<sup>II</sup> cations and their dihedral angle is  $2.38^\circ$ , which indicates that La<sup>III</sup> cations are not fully incorporated into the monovacant site of  $[\alpha\text{-GeW}_{11}\text{O}_{39}]^{8-}$  fragments. This case is not only related to the atom radius of the La<sup>III</sup> cation being larger than that the W center but also is in relation to the bridging role of La<sup>III</sup> cations in the construction of the 1-D linear chain  $\{[\text{Cu}(\text{dap})_2(\text{H}_2\text{O})][\text{La}(\text{H}_2\text{O})_3(\alpha\text{-GeW}_{11}\text{O}_{39})]\}_n^{3n-}$ . In addition, the 1-D double chains in **1** are aligned in the arrangement mode of -AAA- (Fig. 4c and S5†).

It should be pointed out that the design and assembly of metal-involved supramolecular architectures are currently of great interest in supramolecular chemistry and crystal engineering because they can provide novel topology and functional materials.<sup>21</sup> Moreover, Keggin-based supramolecular architectures are regarded as one of the most promising materials potentially applied in the field of chemistry, biology and materials science.<sup>22</sup> From the viewpoint of supramolecular

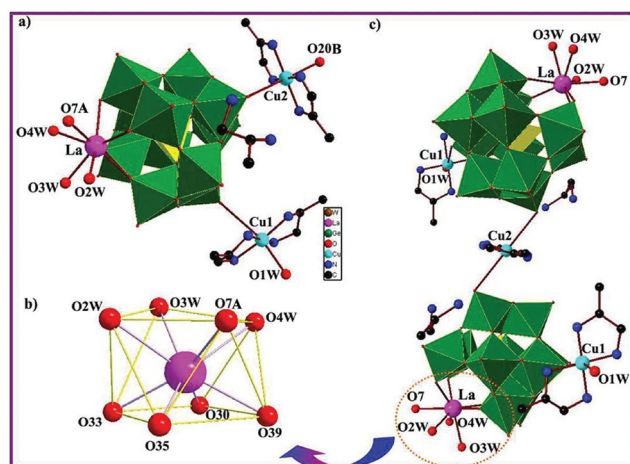


Fig. 3 (a) The asymmetrical structural unit of **1** with the selected numbering scheme; (b) the eight-coordinate distorted square antiprism of the La<sup>III</sup> cation; and (c) the dimeric structural unit made up of two  $[\text{Cu}(\text{dap})_2(\text{H}_2\text{O})][\text{La}(\text{H}_2\text{O})_3(\alpha\text{-GeW}_{11}\text{O}_{39})]^{5-}$  moieties through a  $[\text{Cu}_2(\text{dap})_2]^{2+}$  linker. The atoms with "A, B" labels are symmetrically generated (A:  $1 + x, y, z$ ; B:  $1 - x, 1 - y, -z$ ). Hydrogen atoms, protons and lattice water molecules are omitted for clarity.

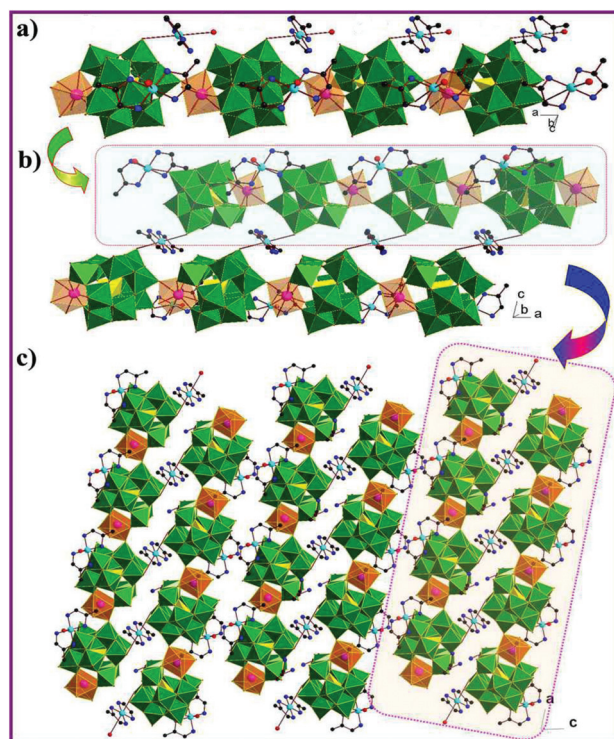


Fig. 4 (a) The 1-D chain constructed by the W-O-La-O7-W linkers in **1**; (b) the 1-D organic-inorganic hybrid double-chain architecture of **1**; and (c) arrangement of 1-D double-chains in the crystallographic ac plane in **1** showing the mode of -AAA-.

chemistry, supramolecular structures are also present in 1–7 considering hydrogen bonding interactions between nitrogen atoms of dap ligands and surface oxygen atoms of POM units and water molecules. Specifically speaking, dap ligands work as the proton donors, surface oxygen atoms of mono-RE substituted Keggin GTs and water molecules function as the proton acceptors, and then donors and acceptors are hydrogen-bonded together generating the infinitely 3-D supramolecular architectures (Fig. 6). The N–H...O distances are in the range of 2.67(3)–3.48(4) Å for 1, 2.859(19)–3.51(2) Å for 2, 2.87(3)–3.54(3) Å for 3, 2.83(4)–3.41(4) Å for 4, 2.64(6)–3.43(5) Å for 5, 2.59(3)–3.47(3) Å for 6, and 2.90(2)–3.35(4) Å for 7, respectively.

### IR spectra

IR spectra for 1–7 were recorded as KBr pellets in the range of 4000–400  $\text{cm}^{-1}$  (Fig. S1A and S1B†). Their IR spectra display the characteristic vibration patterns resulting from the Keggin POT framework in the region of 1100–600  $\text{cm}^{-1}$ . Four characteristic vibration bands attributable to  $\nu_{\text{as}}(\text{Ge}-\text{O}_a)$ , terminal  $\nu_{\text{as}}(\text{W}-\text{O}_t)$ , corner-sharing  $\nu_{\text{as}}(\text{W}-\text{O}_b)$ , and edge-sharing  $\nu_{\text{as}}(\text{W}-\text{O}_c)$  asymmetric vibrations derived from the Keggin GT framework appear at 879–873, 944–940, 814–810, 769–766 and 697–692  $\text{cm}^{-1}$ , respectively. Specifically, four groups of characteristic vibration bands corresponding to  $\nu(\text{Ge}-\text{O}_a)$ ,  $\nu(\text{W}-\text{O}_t)$ ,  $\nu(\text{W}-\text{O}_b)$ , and  $\nu(\text{W}-\text{O}_c)$  are observed at 873; 940; 811; 767; and 692  $\text{cm}^{-1}$  for 1, 876; 939; 813; 767; and 693  $\text{cm}^{-1}$  for 2, 876; 941; 876; 813; 767; and 695  $\text{cm}^{-1}$  for 3, 876; 941; 814; 769; and 695  $\text{cm}^{-1}$  for 4, 875; 942; 810; 766; and 693  $\text{cm}^{-1}$  for 5, 877; 943; 813; 768; and 697  $\text{cm}^{-1}$  for 6, 879; 944; 812; 767; and 695  $\text{cm}^{-1}$  for 7, respectively. In general, these characteristic bands can be easily assigned in comparison with the corresponding bands of monovacant Keggin POT clusters.<sup>15,16a</sup> Compared with the  $\text{K}_6\text{Na}_2[\alpha\text{-GeW}_{11}\text{O}_{39}]\cdot 13\text{H}_2\text{O}$  precursor,<sup>16b</sup> the

$\nu(\text{W}-\text{O}_t)$  vibration bands for 1–7 are almost not shifted, suggesting the weak influence of  $[\text{Cu}(\text{dap})]^{2+}$  and  $[\text{Cu}(\text{dap})_2(\text{H}_2\text{O})]^{2+}$  cations on the terminal oxygen atoms on the  $[\alpha\text{-GeW}_{11}\text{O}_{39}]^{8-}$  fragments. This phenomenon can be also confirmed by the long Cu–O<sub>t</sub> distances (>2.5 Å) from the X-ray single crystal analyses. Furthermore, the possible major reason why the  $\nu(\text{W}-\text{O}_b)$  split into two bands may be related to the fact that the incorporation of the Ln cations into the defect sites of  $[\alpha\text{-GeW}_{11}\text{O}_{39}]^{8-}$  fragments leads to the deformation and distortion of the  $[\alpha\text{-GeW}_{11}\text{O}_{39}]^{8-}$  skeletons. In addition, the stretching bands of –OH, –NH<sub>2</sub> and –CH<sub>2</sub> groups are observed at 3486–3461, 3308–3140 and 2971–2928  $\text{cm}^{-1}$ , respectively. The bending vibration bands of –NH<sub>2</sub> and –CH<sub>2</sub> groups appear at 1621–1522 and 1493–1461  $\text{cm}^{-1}$ , respectively. The occurrence of these characteristic signals confirms the presence of organic amine groups and water molecules in 1–7, which is in good agreement with the single-crystal structural analyses.

### Magnetic properties

Recently, the research and discovery of TM–Ln containing complexes with magnetic interactions in the solid-state chemistry and materials science have been attracting increasing attention.<sup>23</sup> Though lots of TM–Ln containing complexes have been reported, except for the isotropic Gd<sup>III</sup> cation having an  $f^7$  electron configuration and an orbitally non-degenerate ground state, not much is known about the nature and magnitude of the exchange interaction of Ln cations between themselves and with other magnetic groups and the evolution of the magnetic properties along the Ln series,<sup>24a</sup> because the magnetic properties of Ln cations are strongly influenced by spin–orbit couplings and in particular the magnetocrystalline anisotropy is generally large.<sup>24b,c</sup> Generally, the orbital component of the magnetic moment is much more important for Ln cations compared to TM cations, since ligand-field effects are smaller and spin–orbit couplings larger for  $f$  electrons of Ln cations.<sup>25a</sup> Under the influence of the interelectronic repulsion and spin–orbit couplings, the  $^{2S+1}L$  group term of the  $4f^n$  configuration of Ln cations is split into  $^{2S+1}L_J$  spectroscopic levels. Each of these states is further split into Stark sublevels by the ligand-field perturbation.<sup>24a</sup> Although the theory of the paramagnetic properties of Ln cations has long been

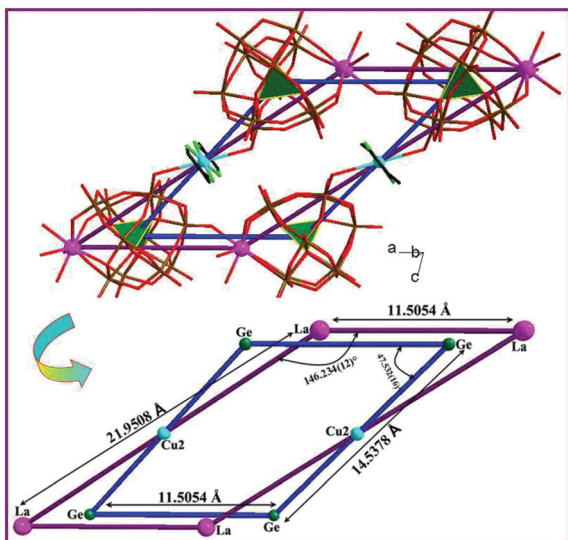


Fig. 5 Two parallelograms in the structure.

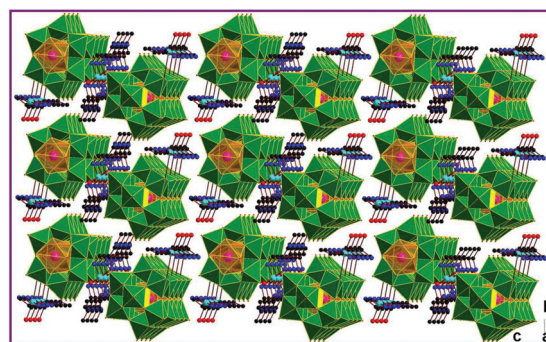


Fig. 6 The 3-D extended supramolecular architecture of 1.



investigated, the presence of a large unquenched orbital angular momentum has not allowed the development of simple models for a rational analysis of the structural magnetic correlations.<sup>24c</sup> Since there are Cu<sup>III</sup> and Ln<sup>III</sup> centers in 1–7, the magnetic susceptibilities of 2, 4 and 7 have been measured on their polycrystalline samples in an applied magnetic field of 2000 Oe in the temperature range of 2–300 K (Fig. 7) on a Quantum Design MPMS XL-7 magnetometer.

In the case of 2, the magnetic data for 2 are plotted in the form of  $\chi_M$  and  $\chi_M T$  versus  $T$  (Fig. 7a). The temperature dependence of  $\chi_M$  exhibits a slight increase from 0.01 emu mol<sup>-1</sup> at 300 K to 0.05 emu mol<sup>-1</sup> at 36 K. This tendency becomes more pronounced below 36 K, exponentially reaching 0.42 emu mol<sup>-1</sup> at 2 K. Correspondingly, the  $\chi_M T$  product at 300 K of 2.29 emu K mol<sup>-1</sup> is consistent with the theoretical value (2.16 emu K mol<sup>-1</sup>) expected for 1.5 non-interacting Cu<sup>II</sup> cations ( $S = 1/2$ ) considering  $g = 2$  and 1 isolated Pr<sup>III</sup> cations ( $^3H_4, J = 4, g = 4/5$ ).<sup>25b</sup> The  $\chi_M T$  value declines gradually between 300 and 34 K, where the  $\chi_M T$  value is 1.69 emu K mol<sup>-1</sup>. Below 34 K, it falls sharply to 0.82 emu K mol<sup>-1</sup> at 2 K. This decline phenomenon is related to the depopulation of the Stark levels of Pr<sup>III</sup> cations upon cooling. It is well known that ligand-field effects can split the 9-fold degenerate  $^3H_4$  ground state of the Pr<sup>III</sup> cation into Stark levels and the value of  $\chi_M T$  mainly depends on the populations of those Stark levels.<sup>25c</sup> As for 2, at 300 K, all the Stark levels from the 9-fold degenerate  $^3H_4$  ground states are populated, such that  $\chi_M T$  is equal to the value expected for one free Pr<sup>III</sup> ion and one and a half isolated Cu<sup>II</sup> cations; however, as temperature drops, progressive depopulation of higher Stark levels occurs, leading to the decrease of the  $\chi_M T$  value. The curve of  $\chi_M^{-1}$  versus  $T$  between 80 and 300 K (Fig. 7b) follows the Curie–Weiss expression [ $\chi_M = C / (T - \theta)$ ] with  $C = 2.44$  emu K mol<sup>-1</sup> and  $\theta = -15.05$  K for 2. The larger  $\theta$  value also indicates the importance of ligand-field effects in 2.<sup>25d</sup> In the meantime, the progressive depopulation of higher Stark levels can also result in the deviation of the curve of  $\chi_M^{-1}$  versus  $T$  to the Curie–Weiss law.

For 4, the magnetic data are plotted in Fig. 7c in the form of  $\chi_M$  and  $\chi_M T$  versus  $T$ . The temperature dependence of  $\chi_M$  exhibits a slight increase from 0.003 emu mol<sup>-1</sup> at 300 K to 0.019 at 36 K and then exponentially to the maximal value of 0.321 emu mol<sup>-1</sup> at 2 K. The  $\chi_M T$  product at 300 K is 0.81 emu K mol<sup>-1</sup>, being higher than the expected value of 0.65 emu K mol<sup>-1</sup> for 1.5 isolated Cu<sup>II</sup> cations with  $S = 1/2$  and  $g = 2$  and 1 free Sm<sup>III</sup> cation ( $^6H_{5/2}, J = 5/2, g = 2/7$ ).<sup>25e</sup> This suggests the existence of the thermal population of the higher energy state of the free Sm<sup>III</sup> ion at room temperature. In general, the  $^6H$  ground term for the free Sm<sup>III</sup> ion in the crystal field is split into six states by spin–orbit coupling and the spin–orbit coupling parameter is 1200 cm<sup>-1</sup>, which often leads to the thermal population of the high energy states.<sup>25f,g</sup> The  $\chi_M T$  value declines from 300 to 2 K, finally reaches the minimum value of 0.64 emu K mol<sup>-1</sup>, which illustrates the occurrence of depopulation of the Kramers doublets of higher energy. Similar phenomena have been observed in the Sm<sup>III</sup>-containing complexes such as [Sm<sub>2</sub>(4-cba)<sub>6</sub>(phen)<sub>2</sub>(H<sub>2</sub>O)<sub>2</sub>] and

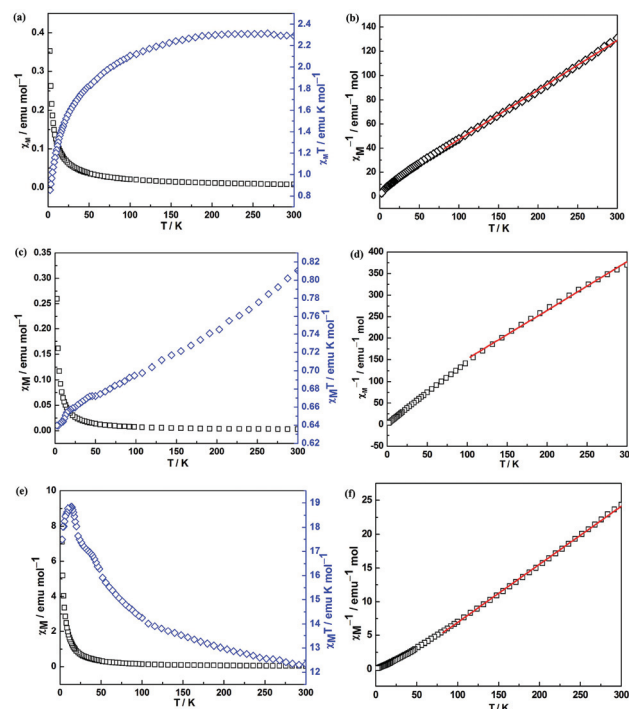


Fig. 7 (a) Temperature dependence of magnetic susceptibility for 2 between 2 and 300 K; (b) temperature evolution of the inverse magnetic susceptibility for 2 between 80 and 300 K; (c) temperature dependence of magnetic susceptibility for 4 between 2 and 300 K; (d) temperature evolution of the inverse magnetic susceptibility for 4 between 100 and 300 K; (e) temperature dependence of magnetic susceptibility for 7 between 2 and 300 K; and (f) temperature evolution of the inverse magnetic susceptibility for 7 between 80 and 300 K. The red solid lines were generated from the best fit by the Curie–Weiss expression.

[{(α-PW<sub>11</sub>O<sub>39</sub>)Ln(H<sub>2</sub>O)(η<sup>2</sup>,μ-1,1)-CH<sub>3</sub>COO]<sub>2</sub>]<sup>10-</sup>.<sup>25c,g</sup> Actually, the curve of  $\chi_M^{-1}$  versus  $T$  in 100–300 K for 4 can be described using the Curie–Weiss law with the  $C = 0.88$  emu K mol<sup>-1</sup> and  $\theta = 33.89$  K (Fig. 7d), but the depopulation of the Kramers doublets of higher energy upon cooling results in the deviation of the relationship of  $\chi_M^{-1}$  versus  $T$  between 100 and 2 K.

With respect to 7, the  $\chi_M$  value slowly increase from 0.04 emu mol<sup>-1</sup> at 300 K to 0.42 emu mol<sup>-1</sup> at 40 K and then exponentially reaches the maximum of 8.50 emu mol<sup>-1</sup> at 2 K (Fig. 7e). The value of  $\chi_M T$  at 300 K of 12.33 emu K mol<sup>-1</sup> is in line with the sum (12.04 emu K mol<sup>-1</sup>) of the contribution attributable to one and a half free Cu<sup>II</sup> cations ( $S = 1/2$ ) with  $g = 2.00$  and one free Er<sup>III</sup> cation in the  $^4I_{15/2}$  group state ( $J = 15/2, g = 6/5$ ).<sup>25h-k</sup> The  $\chi_M T$  value increases to a maximum of 18.85 emu K mol<sup>-1</sup> at 14 K upon cooling (Fig. 7e). This behavior may indicate that the  $S_{Er} = 11/2$  local spins somewhat tend to align along the same direction. The  $\chi_M T$  decreases on decreasing temperature from 14 to 2 K. This behavior suggests the intermolecular interactions. The relationship of  $\chi_M^{-1}$  versus  $T$  in 80–300 K can be described by the Curie–Weiss law with  $C = 11.60$  emu K mol<sup>-1</sup> and  $\theta = -19.63$  K (Fig. 7f). However, as the temperature decreases from 80 to 2 K, the relationship of  $\chi_M^{-1}$  versus  $T$  does not follow the Curie–Weiss law.

## Electrochemical and electrocatalytic properties

POMs, as a large and rapidly growing class, can undergo a reversible multi-electron redox process, and can be utilized as the chemically bulk-modified CPEs with many advantages of inexpensive, easy to handle, and easy to prepare, so they have attracted much attention in electrochemical applications and the manufacture of chemically modified electrodes.<sup>26</sup> By means of cyclic voltammetry (CV), the solid-state electrochemical and electrocatalytic properties of **3** and **4** have been measured in 0.5 mol L<sup>-1</sup> Na<sub>2</sub>SO<sub>4</sub> + H<sub>2</sub>SO<sub>4</sub> aqueous solution (a medium suitable for testing electro-catalytic processes) by entrapping them in a carbon paste electrode (CPE). The reproducibility of cyclic voltammograms indicates that **3**-CPE and **4**-CPE are stable in this medium. Since **3** and **4** are isostructural, their electrochemical and electro-catalytic properties are very similar (Fig. 8 and S6<sup>†</sup>). Since the pH value of the supporting electrolyte has a marked effect on the electrochemical behavior, we find that the best pH values of **3** and **4** are 1.34 and 1.35, respectively (Fig. S7 and S8).<sup>†</sup> Fig. 8a shows the typical CV behavior of **3** in a pH 1.34 sulfate medium (0.5 mol L<sup>-1</sup> Na<sub>2</sub>SO<sub>4</sub> + H<sub>2</sub>SO<sub>4</sub>) at a scan rate of 50 mV s<sup>-1</sup> at room temperature. Considering the same for **4**, its typical CV behavior is illustrated in Fig. S6a.<sup>†</sup> It can be clearly seen that in the potential range of -0.8 to 0.4 V, the CV patterns are restricted to two pairs of redox waves and their mean peak potentials  $E_{1/2} = (E_{pa} + E_{pc})/2$  are -0.613 V and -0.023 V (vs. the Ag/AgCl electrode) for **3** and -0.548 V and 0.007 V (vs. the Ag/AgCl electrode) for **4**, respectively. As expected, the W<sup>VI</sup>-based wave is located at a more negative potential than that attributable to the Cu<sup>II</sup> center. The former features the redox process of the W<sup>VI</sup> centers and the latter is attributed to the redox process of the Cu<sup>II</sup> center in the polyoxoanion framework.<sup>13,26c</sup>

Previous studies have shown that POMs are capable of delivering the electrons to other species, thus serving as powerful electron reservoirs for multi-electron reductions and electrocatalytic processes.<sup>27a</sup> For example, Toth and Anson applied the iron<sup>III</sup>-substituted Keggin type POMs as catalysts in the reductions of hydrogen peroxide and nitrite.<sup>2b</sup> Dong *et al.* observed that [SiW<sub>12</sub>O<sub>40</sub>]<sup>4-</sup> could act as an electrocatalyst for the reduction of nitrite.<sup>27a</sup> Here, **3**-CPE and **4**-CPE are employed to probe the electro-catalytic reductions of hydrogen peroxide, bromate and nitrite in 0.5 mol L<sup>-1</sup> Na<sub>2</sub>SO<sub>4</sub> + H<sub>2</sub>SO<sub>4</sub> aqueous solution (pH = 1.34 for **3** and pH = 1.35 for **4**). The H<sub>2</sub>O<sub>2</sub> electro-activity improvement is of special interest for applications such as the chemical industry, biosensors and fuel cells.<sup>28a</sup> Thus, electro-catalytic investigations on the reduction of hydrogen peroxide catalyzed by other POMs have been performed. For instance, in 2004, Wang's group firstly reported a high electrocatalytic reduction activity of hydrogen peroxide catalyzed by the Keggin-type phosphomolybdate (PMo<sub>12</sub>)-doped polypyrrole (PPy) CPE.<sup>28b</sup> In order to evaluate the electrocatalytic activity, **3**-CPE and **4**-CPE are employed to probe the electrocatalytic reduction of hydrogen peroxide (Fig. 8b and S6b<sup>†</sup>). As shown in Fig. 8b and S6b,<sup>†</sup> with the addition of hydrogen peroxide, the W<sup>VI</sup>-based reduction peak

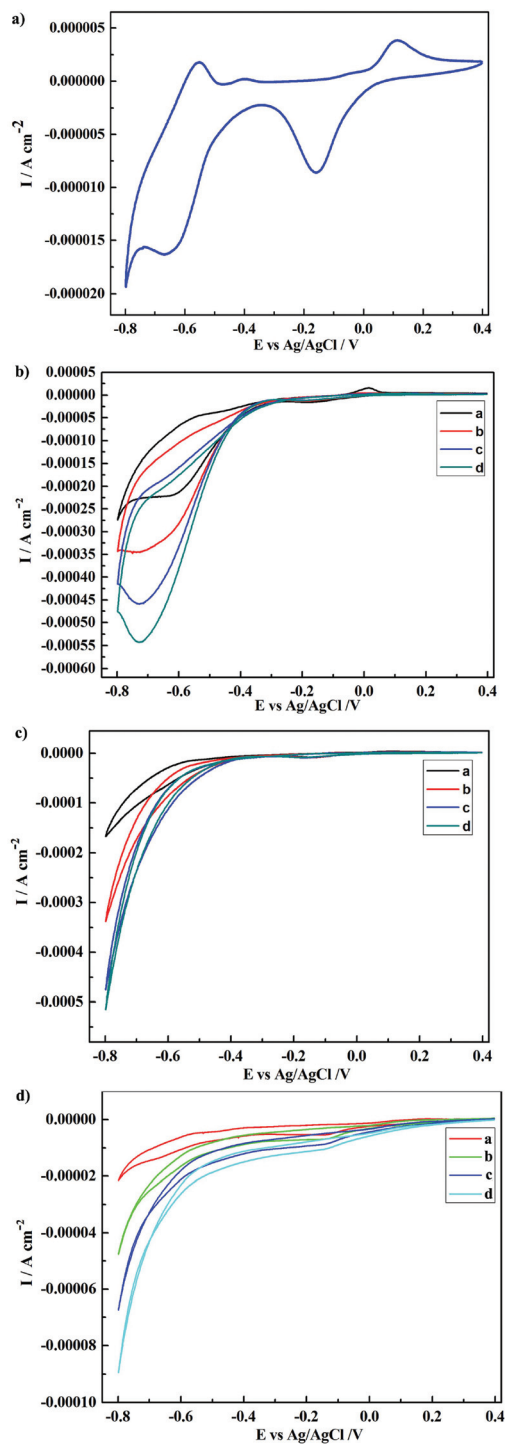


**Fig. 8** (a) Cyclic voltammogram of **3**-CPE in pH = 1.34 0.5 mol L<sup>-1</sup> Na<sub>2</sub>SO<sub>4</sub> + H<sub>2</sub>SO<sub>4</sub> aqueous solution; (b) the evolution of cyclic voltammograms of **3**-CPE in pH = 1.34 0.5 mol L<sup>-1</sup> Na<sub>2</sub>SO<sub>4</sub> + H<sub>2</sub>SO<sub>4</sub> aqueous solution containing various H<sub>2</sub>O<sub>2</sub> concentrations (a 5.88 × 10<sup>-3</sup>, b 9.80 × 10<sup>-3</sup>, c 1.37 × 10<sup>-2</sup>, d 1.76 × 10<sup>-2</sup> mol L<sup>-1</sup>); (c) the evolution of cyclic voltammograms of **3**-CPE in pH = 1.34 0.5 mol L<sup>-1</sup> Na<sub>2</sub>SO<sub>4</sub> + H<sub>2</sub>SO<sub>4</sub> aqueous solution containing various NaBrO<sub>3</sub> concentrations (a 1 × 10<sup>-3</sup>, b 3 × 10<sup>-3</sup>, c 5 × 10<sup>-3</sup>, d 7 × 10<sup>-3</sup>); and (d) the evolution of cyclic voltammograms of **3**-CPE in pH = 1.34 0.5 mol L<sup>-1</sup> Na<sub>2</sub>SO<sub>4</sub> + H<sub>2</sub>SO<sub>4</sub> aqueous solution containing various NaNO<sub>2</sub> concentrations (a 3 × 10<sup>-3</sup>, b 5 × 10<sup>-3</sup>, c 7 × 10<sup>-3</sup>, d 9 × 10<sup>-3</sup> mol L<sup>-1</sup>). Scan rate: 50 mV s<sup>-1</sup>.

currents increase, while the corresponding oxidation peak currents decrease. However, the  $\text{Cu}^{\text{II}}$  reduction wave is almost unaffected by addition of hydrogen peroxide. The results show that the reduction of nitrite is mainly mediated by the reduced species of tungsten-oxo clusters in **3** and **4**. To further illustrate their electrocatalytic potential, the reduction procedures of bromate catalyzed by them have been also carried out. The monitoring or removal of bromate species is interesting as it is present in drinking water samples as a byproduct of ozone disinfection and is often used as a food additive.<sup>12b</sup> Moreover, the negative impacts of bromate on the human body have been confirmed.<sup>28c</sup> As a result, developing new, rapid and inexpensive analytic methods to detect the presence of bromate is indispensable. So the electrocatalytic abilities of **3**-CPE and **4**-CPE toward the reduction of  $\text{BrO}_3^-$  have been studied in  $0.5 \text{ mol L}^{-1} \text{ Na}_2\text{SO}_4 + \text{H}_2\text{SO}_4$  aqueous solution containing various  $\text{NaBrO}_3$  concentrations at room temperature. Fig. 8c and S6c† show the cyclic voltammograms for the electrocatalytic reduction of bromate by **3**-CPE and **4**-CPE. The catalytic effects of  $\text{BrO}_3^-$  are similar to the  $\text{H}_2\text{O}_2$  for **3** and **4**, with addition of  $\text{NaBrO}_3$ , the reduction peak currents of the  $\text{Cu}^{\text{II}}$ -based wave is less affected whereas the  $\text{W}^{\text{VI}}$ -based reduction peak currents increase gradually and the corresponding oxidation peak currents gradually decrease, suggesting that the bromate is reduced by the species of tungsten components.<sup>28d</sup> Actually, such a phenomenon has been previously encountered.<sup>12b,28e,f</sup> In addition, the electrocatalytic reduction of nitrite on **3**-CPE and **4**-CPE is also measured. The catalytic reduction evolution of nitrite on **3**-CPE and **4**-CPE can be seen clearly in Fig. 8d and S6d.† Unlike the electrocatalytic reductions of hydrogen peroxide and bromate, the electrocatalytic reductions not only occur on the  $\text{W}^{\text{VI}}$ -based wave obviously, but also appear on the  $\text{Cu}^{\text{II}}$ -based wave. With addition of  $\text{NaNO}_2$ , the reduction peak currents of the  $\text{W}^{\text{VI}}$ -based wave and  $\text{Cu}^{\text{II}}$ -based wave increase steadily and their corresponding oxidation peak currents decrease. The results show that the electrocatalytic reduction of nitrite is simultaneously mediated by the  $\text{W}^{\text{VI}}$ -based wave and  $\text{Cu}^{\text{II}}$ -based wave in **3** and **4**. As discussed above, **3** and **4** display apparent electro-catalytic activities for the nitrite, bromate and hydrogen peroxide reduction.

## Conclusions

In conclusion, we have synthesized a family of 1-D double chain organic-inorganic hybrid Cu-Ln heterometallic GTs  $[\text{H}_2\text{dap}][\text{Cu}(\text{dap})_2(\text{H}_2\text{O})][\text{Cu}(\text{dap})_2]_{0.5}[\text{Ln}(\text{H}_2\text{O})_3(\alpha\text{-GeW}_{11}\text{O}_{39})] \cdot 3\text{H}_2\text{O}$  [Ln =  $\text{La}^{\text{III}}$  (**1**),  $\text{Pr}^{\text{III}}$  (**2**),  $\text{Nd}^{\text{III}}$  (**3**),  $\text{Sm}^{\text{III}}$  (**4**),  $\text{Eu}^{\text{III}}$  (**5**),  $\text{Tb}^{\text{III}}$  (**6**),  $\text{Er}^{\text{III}}$  (**7**)] under hydrothermal conditions, which are structurally characterized by elemental analyses, IR spectra, PXRD, TG analyses, XPS and single-crystal X-ray diffraction. X-ray diffraction structural analyses indicate that **1**-**7** are isomorphic and adopt novel 1-D double-chain architectures constructed by two antiparallel 1-D polymeric chains linked through  $[\text{Cu}(\text{dap})_2]^{2+}$  linkages. As far as we know, they exemplify a rare type of organic-inorganic hybrid 1-D double chain Cu-Ln

heterometallic GTs. The magnetic properties of **2**, **4** and **7** have been measured and their magnetic behaviors are mainly affected by Ln centers with a strong spin-orbit coupling contribution and/or the ligand-field perturbation. The TG curves of **2**, **5**, **6** and **7** show two steps of weight loss between 25 and 700 °C. Furthermore, the solid-state electrochemical and electro-catalytic properties of **3** and **4** have been evaluated. The electrocatalytic reductions of hydrogen peroxide and bromate are principally mediated by the  $\text{W}^{\text{VI}}$ -based wave while the reduction of nitrite is simultaneously mediated by the  $\text{W}^{\text{VI}}$ -based wave and  $\text{Cu}^{\text{II}}$ -based wave. In short, **3**-CPE and **4**-CPE have obvious electro-catalytic activities for the reductions of hydrogen peroxide, bromate and nitrite. The key points of the synthetic procedures have been well established. In the future, other functional organic ligands such as aliphatic polycarboxylic acid, aromatic polycarboxylic acid and amino acid ligands will be introduced into this system to make TM-Ln cluster substituted GTs with novel architectures and excellent functional properties. It can be believed that these findings are very significant in exploring the syntheses of organic-inorganic hybrid TM-Ln heterometallic GTs, even for PBTLDs.

## Acknowledgements

This work was supported by the Natural Science Foundation of China (21101055, 21301049, U1304208), China Postdoctoral Science Foundation Funded Project (201104392, 20100470996), the Natural Science Foundation of Henan Province (122300410106, 102300410093), the Foundation of State Key Laboratory of Structural Chemistry (20120013), 2012 Young Backbone Teachers Foundation from Henan Province and the 2012, 2013 Students Innovative Pilot Plans of Henan University.

## References

- (a) M. T. Pope, *Heteropoly and Isopoly Oxometalates*, Springer-Verlag, Berlin, Germany, 1983; (b) J. J. Borrás-Almenar, E. Coronado, A. Müller and M. T. Pope, *Polyoxometalate Molecular Science*, Kluwer Academic Publishers, Dordrecht, The Netherlands, 2003; (c) M. AlDamen, J. Clemente-Juan, E. Coronado, C. Martí-Gastaldo and A. Gaita-Ariño, *J. Am. Chem. Soc.*, 2008, **130**, 8847; (d) C. Ritchie, A. Ferguson, H. Nojiri, H. N. Miras, Y. F. Song, D. L. Long, E. Burkholder, M. Murrie, P. Kögerler, E. Brechin and L. Cronin, *Angew. Chem., Int. Ed.*, 2008, **47**, 5609; (e) A. Dolbecq, E. Dumas, L. C. Francescino and M. R. Antonio, *Inorg. Chem.*, 2008, **47**, 6889.
- (a) B. Godin, Y. Chen, J. Vaissermann, L. Ruhlmann, M. Verdager and P. Gouzerh, *Angew. Chem., Int. Ed.*, 2005, **44**, 3072; (b) S. S. Mal and U. Kortz, *Angew. Chem., Int. Ed.*, 2005, **44**, 3777; (c) G. S. Kim, H. D. Zeng, D. Van Derveer and C. L. Hill, *Angew. Chem., Int. Ed.*, 1999, **38**, 3205;



- (d) Y. Sakai, K. Yoza, C. N. Kato and K. Nomiya, *Chem.–Eur. J.*, 2003, **9**, 4077; (e) S. T. Zheng, J. Zhang, J. M. Clemente-Juan, D. Q. Yuan and G. Y. Yang, *Angew. Chem., Int. Ed.*, 2009, **48**, 7176; (f) B. S. Bassil, M. Ibrahim, R. Al-Oweini, M. Asano, Z. Wang, J. van Tol, N. S. Dalal, K. Y. Choi, R. N. Biboum, B. Keita, L. Nadjo and U. Kortz, *Angew. Chem., Int. Ed.*, 2011, **50**, 5961; (g) P. I. Molina, H. N. Miras, D. L. Long and L. Cronin, *Inorg. Chem.*, 2013, **52**, 9284.
- 3 (a) T. Yamase, *Chem. Rev.*, 1998, **98**, 307; (b) C. Benelli and D. Gatteschi, *Chem. Rev.*, 2002, **102**, 2369; (c) H. E. Moll, B. Nohra, P. Mialane, J. Marrot, N. Dupré, B. Riffade, M. Malacria, S. Thorimbek, B. Hasenknopf, E. Lacôte, P. A. Aparicio, X. López, J. M. Poblet and A. Dolbecq, *Chem.–Eur. J.*, 2011, **17**, 14129; (d) Y. Kikukawa, S. Yamaguchi, K. Tsuchida, Y. Nakagawa, K. Uehara, K. Yomaguchi and N. Mizuho, *J. Am. Chem. Soc.*, 2008, **130**, 5472; (e) C. Boglio, G. Lemiére, B. Hasenknopf, S. Thorimbert, E. Lacôte and M. Malacria, *Angew. Chem., Int. Ed.*, 2006, **45**, 3324.
- 4 (a) K. Wassermann, M. H. Dickman and M. T. Pope, *Angew. Chem., Int. Ed. Engl.*, 1997, **36**, 1445; (b) R. C. Howell, F. G. Perez, S. Jain, W. D. Horrocks Jr., A. L. Rheingold and L. C. Francesconi, *Angew. Chem., Int. Ed.*, 2001, **40**, 4031; (c) G. L. Xue, J. Vaissermann and P. Gouzerh, *J. Cluster Sci.*, 2002, **13**, 409; (d) K. Fukaya and T. Yamase, *Angew. Chem., Int. Ed.*, 2003, **42**, 654; (e) B. S. Bassil, M. H. Dickman, I. Römer, B. von der Kammer and U. Kortz, *Angew. Chem., Int. Ed.*, 2007, **46**, 6192; (f) F. Hussain, F. Conrad and G. R. Patzke, *Angew. Chem. Int. Ed.*, 2009, **48**, 9088.
- 5 H. Y. An, Y. Lan, Y. G. Li, E. B. Wang, N. Hao, D. R. Xiao, L. Y. Duan and L. Xu, *Inorg. Chem. Commun.*, 2004, **7**, 356.
- 6 (a) J. D. Compain, P. Mialane, A. Dolbecq, I. M. Mbomekallé, J. Marrot, F. Sécheresse, C. Duboc and E. Rivière, *Inorg. Chem.*, 2010, **49**, 2851; (b) X. J. Feng, W. Z. Zhou, Y. G. Li, H. S. Ke, J. K. Tang, R. Clérac, Y. H. Wang, Z. M. Su and E. B. Wang, *Inorg. Chem.*, 2012, **51**, 2722; (c) D. Y. Shi, J. W. Zhao, L. J. Chen, P. T. Ma, J. P. Wang and J. Y. Niu, *CrystEngComm*, 2012, **14**, 3108.
- 7 (a) C. D. Wu, C. Z. Lu, H. H. Zhuang and J. S. Huang, *J. Am. Chem. Soc.*, 2002, **124**, 3836; (b) P. Mialane, A. Dolbecq, E. Rivière, J. Marrot and F. Sécheresse, *Eur. J. Inorg. Chem.*, 2004, **33**.
- 8 S. Reinoso, *Dalton Trans.*, 2011, **40**, 6610.
- 9 (a) W. L. Chen, Y. G. Li, Y. H. Wang and E. B. Wang, *Eur. J. Inorg. Chem.*, 2007, 2216; (b) X. K. Fang and P. Kögerler, *Angew. Chem., Int. Ed.*, 2008, **47**, 8123; (c) X. K. Fang and P. Kögerler, *Chem. Commun.*, 2008, 3396; (d) W. L. Chen, Y. G. Li, Y. G. Wang, E. B. Wang and Z. M. Zhang, *Dalton Trans.*, 2008, 865; (e) J. F. Cao, S. X. Liu, R. G. Cao, L. H. Xie, Y. H. Ren, C. Y. Gao and L. Xu, *Dalton Trans.*, 2008, 115; (f) B. Nohra, P. Mialane, A. Dolbecq, E. Rivière, J. Marrot and F. Sécheresse, *Chem. Commun.*, 2009, 2703; (g) Y. W. Li, Y. G. Li, Y. H. Wang, X. J. Feng, Y. Lu and E. B. Wang, *Inorg. Chem.*, 2009, **48**, 6452; (h) D. Y. Du, J. S. Qin, S. L. Li, Y. Q. Lan, X. L. Wang and Z. M. Su, *Aust. J. Chem.*, 2010, **63**, 1389; (i) S. Yao, Z. M. Zhang, Y. G. Li, Y. Lu, E. B. Wang and Z. M. Su, *Cryst. Growth Des.*, 2010, **10**, 135; (j) J. Y. Niu, S. W. Zhang, H. N. Chen, J. W. Zhao, P. T. Ma and J. P. Wang, *Cryst. Growth Des.*, 2011, **11**, 3769; (k) Z. M. Zhang, Y. G. Li, S. Yao and E. B. Wang, *Dalton Trans.*, 2011, **40**, 6475; (l) S. W. Zhang, J. W. Zhao, P. T. Ma, J. Y. Niu and J. P. Wang, *Chem.–Asian J.*, 2012, **7**, 966; (m) A. H. Ismail, B. S. Bassil, G. H. Yassin, B. Keita and U. Kortz, *Chem.–Eur. J.*, 2012, **18**, 6163; (n) H. Y. Zhao, J. W. Zhao, B. F. Yang, H. He and G. Y. Yang, *CrystEngComm*, 2013, **15**, 5209; (o) H. H. Wu, S. Yao, Z. M. Zhang, Y. G. Li, Y. Song, Z. J. Liu, X. B. Han and E. B. Wang, *Dalton Trans.*, 2013, **42**, 342.
- 10 (a) S. Reinoso and J. R. Galán-Mascarós, *Inorg. Chem.*, 2010, **49**, 377; (b) S. Reinoso, J. R. Galán-Mascarós and L. Lezama, *Inorg. Chem.*, 2011, **50**, 9587; (c) S. Reinoso, M. Giménez-Marqués, J. R. Galán-Mascarós, P. Vitoria and J. M. Gutiérrez-Zorrilla, *Angew. Chem., Int. Ed.*, 2010, **49**, 8384.
- 11 U. Kortz, S. Nellutla, A. C. Stowe, N. S. Dalal, U. Rauwald, W. Danquah and D. Ravot, *Inorg. Chem.*, 2004, **43**, 2308.
- 12 (a) J. W. Zhao, D. Y. Shi, L. J. Chen, Y. Z. Li, P. T. Ma, J. P. Wang and J. Y. Niu, *Dalton Trans.*, 2012, **41**, 10740; (b) J. W. Zhao, D. Y. Shi, L. J. Chen, P. T. Ma, J. P. Wang, J. Zhang and J. Y. Niu, *Cryst. Growth Des.*, 2013, **13**, 4368.
- 13 L. H. Bi, U. Kortz, S. Nellutla, A. C. Stowe, J. van Tol, N. S. Dalal, B. Keita and L. Nadjo, *Inorg. Chem.*, 2005, **44**, 896.
- 14 (a) G. M. Sheldrick, *SHELXS 97, Program for Crystal Structure Solution*, University of Göttingen, Göttingen, Germany, 1997; (b) G. M. Sheldrick, *SHELXL 97, Program for Crystal Structure Refinement*, University of Göttingen, Germany, 1997.
- 15 (a) W. J. Niu, D. Y. Shi, J. W. Zhao, X. M. Cai and L. J. Chen, *Inorg. Chem. Commun.*, 2012, **17**, 79; (b) L. J. Chen, D. Y. Shi, J. W. Zhao, Y. L. Wang, P. T. Ma and J. Y. Niu, *Inorg. Chem. Commun.*, 2011, **14**, 1052.
- 16 (a) B. Li, J. W. Zhao, S. T. Zheng and G. Y. Yang, *J. Cluster Sci.*, 2009, **20**, 503; (b) N. Haraguchi, Y. Okaue, T. Isobe and Y. Matsuda, *Inorg. Chem.*, 1994, **33**, 1015.
- 17 (a) I. D. Brown and D. Altermatt, *Acta Crystallogr., Sect. B: Struct. Sci.*, 1985, **41**, 244; (b) A. Trzesowska, R. Kruszynski and J. T. Bartczak, *Acta Crystallogr., Sect. B: Struct. Sci.*, 2004, **60**, 174; (c) N. E. Brese and M. O. Keefe, *Acta Crystallogr., Sect. B: Struct. Sci.*, 1991, **47**, 192.
- 18 (a) H. Martinez, A. Benayad, D. Gonbeau, P. Vinatier, B. Pecquenard and A. Levasseur, *Appl. Surf. Sci.*, 2004, **236**, 377; (b) I. M. Szilágyi, F. Hange, J. Madarász and G. Pokol, *Eur. J. Inorg. Chem.*, 2006, 3413; (c) O. Y. Khyzhuna, T. Strunskusb, S. Cramme and Y. M. Solonina, *J. Alloys Compd.*, 2005, **389**, 14; (d) K. Yu, Y. G. Li, B. B. Zhou, Z. H. Su, Z. F. Zhao and Y. N. Zhang, *Eur. J. Inorg. Chem.*, 2007, 5662; (e) V. B. Kumar, R. Velchuri, V. R. Devi, B. Sreedhar, G. Prasad, D. J. Prakash, M. Kanagaraj, S. Arumugam and M. Vithal, *J. Solid State Chem.*, 2011, **184**,

- 264; (f) T. Akitsu and Y. Einaga, *Polyhedron*, 2006, **25**, 2655; (g) R. Vercaemst, D. Poelman, L. Fiermans, R. L. Van Meirhaeghe, W. H. Laflère and F. Cardon, *J. Electron Spectrosc. Relat. Phenom.*, 1995, **74**, 45.
- 19 B. Li, J. W. Zhao, S. T. Zhen and G. Y. Yang, *Inorg. Chem.*, 2009, **48**, 8294.
- 20 (a) M. Sadakane, M. H. Dickman and M. T. Pope, *Angew. Chem., Int. Ed.*, 2000, **39**, 2914; (b) P. Mialane, L. Lisnard, A. Mallard, J. Marrot, E. Antic-Fidancev, P. Aschehoug, D. Vivien and F. Sécheresse, *Inorg. Chem.*, 2003, **42**, 2102; (c) J. Y. Niu, J. W. Zhao and J. P. Wang, *Inorg. Chem. Commun.*, 2004, **7**, 876; (d) J. P. Wang, X. Y. Duan, X. D. Du and J. Y. Niu, *Cryst. Growth Des.*, 2006, **6**, 2266; (e) J. P. Wang, J. W. Zhao, X. Y. Duan and J. Y. Niu, *Cryst. Growth Des.*, 2006, **6**, 507; (f) J. D. Compain, P. Mialane, A. Dolbecq, I. M. Mbomekallé, J. Marrot, F. Sécheresse, C. Duboc and E. Rivière, *Inorg. Chem.*, 2010, **49**, 2851.
- 21 (a) O. M. Yaghi, M. O'Keeffe, N. W. Ockwig, H. K. Chae, M. Eddaoudi and J. Kim, *Nature*, 2003, **423**, 705; (b) B. Moulton and M. J. Zaworotko, *Chem. Rev.*, 2001, **101**, 1629.
- 22 (a) E. Coronado and C. J. Gómez-García, *Chem. Rev.*, 1998, **98**, 273; (b) P. Q. Zheng, Y. P. Ren, L. S. Long, R. B. Huang and L. S. Zheng, *Inorg. Chem.*, 2005, **44**, 1190; (c) J. W. Zhao, S. T. Zheng and G. Y. Yang, *J. Solid State Chem.*, 2008, **181**, 2205.
- 23 (a) O. Kahn, *Molecular Magnetism*, VCH, Weinheim, 1993; (b) S. Wang, Z. Pang, K. D. L. Smith and M. J. Wanger, *J. Chem. Soc., Dalton Trans.*, 1994, 955; (c) O. Kahn, *Adv. Inorg. Chem.*, 1995, **43**, 179; (d) A. C. Rizzi, R. Calvo, R. Baggio, M. T. Garland, O. Peña and M. Perec, *Inorg. Chem.*, 2002, **41**, 5609.
- 24 (a) M. L. Kahn, J. Sutter, S. Golhen, P. Cuionneau, L. Ouahab, O. Kahn and D. Chasseau, *J. Am. Chem. Soc.*, 2000, **122**, 3413; (b) Y. Q. Sun, J. Zhang, Y. M. Chen and G. Y. Yang, *Angew. Chem., Int. Ed.*, 2005, **44**, 5814; (c) S. W. Zhang, Y. Wang, J. W. Zhao, P. T. Ma, J. P. Wang and J. Y. Niu, *Dalton Trans.*, 2012, **41**, 3764.
- 25 (a) C. Benelli and D. Gatteschi, *Chem. Rev.*, 2002, **102**, 2369; (b) T. Peristeraki, M. Samios, M. Siczek, T. Lis and C. J. Milios, *Inorg. Chem.*, 2011, **50**, 5175; (c) Y. Li, F. K. Zheng, X. Liu, W. Q. Zou, G. C. Guo, C. Z. Lu and J. S. Huang, *Inorg. Chem.*, 2006, **45**, 6308; (d) J. K. Tang, Y. Z. Li, Q. L. Wang, E. Q. Gao, D. Z. Liao, Z. H. Jiang, S. P. Yan, P. Cheng, L. F. Wang and G. L. Wang, *Inorg. Chem.*, 2002, **41**, 2188; (e) T. Arumuganathan and S. K. Das, *Inorg. Chem.*, 2009, **48**, 496; (f) M. Andruh, E. Bakalbassis, O. Kahn, J. C. Trombe and P. Porcher, *Inorg. Chem.*, 1993, **32**, 1616; (g) J. Y. Niu, K. H. Wang, H. N. Chen, J. W. Zhao, P. T. Ma, J. P. Wang, M. X. Li, Y. Bai and D. B. Dang, *Cryst. Growth Des.*, 2009, **9**, 4362; (h) M. L. Kahn, R. Ballou, P. Porcher, O. Kahn and J. P. Sutter, *Chem.-Eur. J.*, 2002, **8**, 525; (i) A. Caneschi, A. Dei, D. Gatteschi, S. Poussereau and L. Sorace, *Dalton Trans.*, 2004, 1048; (j) X. Feng, J. S. Zhao, B. Liu, L. Y. Wang, S. Ng, G. Zhang, J. G. Wang, X. G. Shi and Y. Y. Liu, *Cryst. Growth Des.*, 2010, **10**, 1399; (k) Z. H. Zhang, Y. Song, T. A. Okamura, Y. Hasegawa, W. Y. Sun and N. Uwyama, *Inorg. Chem.*, 2006, **45**, 2896.
- 26 (a) J. E. Toth and F. C. Anson, *J. Am. Chem. Soc.*, 1989, **111**, 2444; (b) X. L. Wang, Z. H. Kang, E. B. Wang and C. W. Hu, *Mater. Lett.*, 2002, **56**, 393; (c) Z. Zhang, Y. Qi, C. Qin, Y. Li, E. Wang, X. Wang, Z. Su and L. Xu, *Inorg. Chem.*, 2007, **46**, 8162.
- 27 (a) S. Dong, X. Xi and M. Tian, *J. Electroanal. Chem.*, 1995, **385**, 227; (b) J. E. Toth and F. C. Anson, *J. Electroanal. Chem.*, 1988, **256**, 361.
- 28 (a) J. Wang, Y. Lin and L. Chen, *Analyst*, 1993, **118**, 277; (b) X. L. Wang, H. Zhang, E. B. Wang, Z. B. Han and C. W. Hu, *Mater. Lett.*, 2004, **58**, 1661; (c) Z. F. Li, J. H. Chen, D. W. Pan, W. Y. Tao, L. H. Nie and S. Z. Yao, *Electrochim. Acta*, 2006, **51**, 4255; (d) H. J. Pang, J. Peng, J. Q. Sha, A. X. Tian, P. P. Zhang, Y. Chen and M. Zhu, *J. Mol. Struct.*, 2009, **921**, 289; (e) B. Keita, P. de Oliveira, L. Nadjo and U. Kortz, *Chem.-Eur. J.*, 2007, **13**, 5480; (f) X. Wang, H. Hu, A. Tian, H. Lin and J. Li, *Inorg. Chem.*, 2010, **49**, 10299.